Loss of genome maintenance accelerates podocyte damage

Fabian Braun[1,2]*, Amrei M. Mandel[1,3,4], Linda Blomberg[1,3], Milagros N. Wong[2], Georgia Chatzinikolaou[5], Viji Nair[6], Roman Akbar-Haase[1,3], Victor G. Puelles[2], Phillip J. McCown[6], Fabian Haas[2], Mahdieh Rahmatollahi[1,3], Damian Fermin[8], Gisela G. Slaats[1,3], Tillmann Bork[9], Christoph Schell[9,10], Sybille Koehler[1,2], Paul T. Brinkoetter[1,3], Maja T. Lindenmeyer[2], Clemens D. Cohen[2,11], Martin Kann[1,3], Wilhelm Bloch[12], Matthew G. Sampson[13,14,15], Martijn ET Dollé[16], Matthias Kretzler[6], George A. Garinis[5,17], Tobias B. Huber[2], Bernhard Schermer[1,3,18], Thomas Benzing[1,3,18], Björn Schumacher[3,17,19], and Christine E. Kurschat[1,3]*

[1]Department II of Internal Medicine and Center for Molecular Medicine Cologne, University of Cologne, Faculty of Medicine and University Hospital Cologne, Cologne, Germany
[2]III. Department of Medicine, University Medical Center Hamburg-Eppendorf, Hamburg, Germany
[3]Cologne Excellence Cluster on Cellular Stress Responses in Aging-Associated Diseases (CECAD), University of Cologne, Faculty of Medicine and University Hospital Cologne, Cologne, Germany
[4]Research Center On Rare Kidney Diseases (RECORD), University Hospital Erlangen, Erlangen, Germany
[5]Institute of Molecular Biology and Biotechnology, Foundation for Research and Technology-Hellas, Heraklion, Crete, Greece.
[6]Division of Nephrology, Department of Internal Medicine, University of Michigan, Ann Arbor, Michigan, USA.
[7] Department of Clinical Medicine, Aarhus University, Aarhus, Denmark
[8]Department of Pediatrics-Nephrology, University of Michigan, Ann Arbor, Michigan
[9]Department of Medicine IV, Faculty of Medicine, University of Freiburg, Freiburg, Germany.
[10]Institute of Surgical Pathology, Faculty of Medicine, University of Freiburg, Freiburg, Germany.
[11]Nephrological Center, Medical Clinic and Polyclinic IV, University of Munich, Munich, Germany
[12]Department of Molecular and Cellular Sport Medicine, German Sport University Cologne, Cologne, Germany
[13]Division of Nephrology, Boston Children's Hospital, Boston, Massachusetts, USA
[14]Harvard Medical School, Boston Massachusetts, USA
[15]Broad Institute, Cambridge, Massachusetts, USA
[16]National Institute for Public Health and the Environment, Bilthoven, The Netherlands.
[17]Department of Biology, University of Crete, Heraklion, Crete, Greece.
[18]Systems Biology of Ageing Cologne, SyBaCol, University of Cologne, Germany
[19]Institute for Genome Stability in Aging and Disease, Medical Faculty, University of Cologne, Germany

Correspondence should be addressed to:

Christine E. Kurschat
Nephrology Research Lab
CECAD
University of Cologne
Joseph Stelzmann-Straße 26
50931 Cologne, Germany
Tel +49-221-478 4480
Fax +49-221-478 5959
E-mail: christine.kurschat@uk-koeln.de

Fabian Braun
E-mail: fa.braun@uke.de
Twitter: @fab_braun

Word count Abstract: 273
Word count Text: 4013

Abstract:

Background: DNA repair is essential for preserving genome integrity and ensuring cellular functionality and survival. Podocytes have a very limited regenerative capacity, and their survival is essential to maintain kidney function. While podocyte depletion is a hallmark of many glomerular diseases, the mechanisms leading to severe podocyte injury and loss remain unclear.

Methods: We investigated DNA repair mechanisms in glomerular diseases by gene expression analysis of human kidney biopsies. Using a constitutive and an inducible podocyte-specific *Ercc1* knockout mouse model, we assessed the influence of disrupted NER *in vivo,* complemented by mechanistical *in vitro* studies of induced DNA damage in cultured podocytes. Furthermore, we characterized DNA damage-related alterations in aged mice and human renal tissue of different age groups as well as in minimal change disease (MCD) and Focal segmental glomerulosclerosis (FSGS) patient biopsies.

Results: We detected perturbed NER gene expression in nuclei of podocytes in FSGS as well as aberrations of DNA repair genes in biopsies of patients with various podocyte-related glomerular diseases. Genome maintenance through NER proved to be indispensable for podocyte homeostasis. Podocyte-specific accumulation of DNA damage through the knockout of the NER endonuclease co-factor Ercc1 resulted in proteinuria, podocyte loss, glomerulosclerosis, and renal insufficiency. The response to this genomic stress was fundamentally different to the pattern reported in other cell types, as podocytes activated mTORC1 signaling upon DNA damage *in vitro* and *in vivo*. The induced mTORC1 activation was abrogated by inhibiting DNA damage response through DNA-PK and ATM *in vitro*. Moreover, pharmacological inhibition of mTORC1 ameliorated the development of glomerulosclerosis in NER-deficient mice.

Conclusion: Disruption of DNA damage response pathways seems to be a uniform response in several glomerulopathies. Accumulation of DNA damage in podocytes results in glomerulosclerosis and activates mTORC1 signaling.

Keywords:

Podocyte, DNA Damage, Ercc1, mTORC1, Glomerulosclerosis

Translational statement

Growing evidence suggests that perturbations in genome maintenance play a role in glomerulopathies. The authors have identified several DNA repair genes to be differentially expressed in glomerular diseases in human kidney biopsies and observed dramatic differences in

90 nucleotide excision repair (NER) gene expression in focal segmental glomerulosclerosis (FSGS)
91 podocytes. *In vivo* and *in vitro* analyses in murine podocytes uncovered accumulation of DNA
92 damage through disruption of NER to result in podocyte loss with glomerulosclerosis and to
93 activate the mTORC1 pathway. Similar results were identified in FSGS patient biopsies as well as
94 in renal specimens of human and murine aging. These findings reveal that DNA damage and its
95 repair pathways are crucial for podocyte maintenance and for the development of
96 glomerulosclerosis, potentially serving as therapeutic targets in the future.
97
98

99 **Introduction:**

100 Most cells of the body are constantly subjected to various endogenous and exogenous DNA
101 damaging agents [1,2]. Therefore, cells depend on numerous DNA repair mechanisms to counteract
102 genomic stress [3]. Mutations in DNA repair genes result in a variety of pathologies ranging from
103 cancer to progeroid syndromes [4,5]. The specific importance of genome maintenance in cells with
104 limited regenerative capacity is demonstrated by the prevalence of neurodegeneration as a
105 hallmark of DNA repair deficiency syndromes [6].

106 Glomerular podocytes are terminally differentiated, post-mitotic cells with little to no replacement
107 post-development [7]. As an integral part of the primary filtration unit of the kidney [8], podocyte
108 depletion is a leading cause of chronic kidney disease due to diabetes, hypertension, and other
109 glomerulopathies, with ensuing loss of protein into the urine [9]. The precise pathomechanisms
110 leading to podocyte depletion, however, are incompletely understood. Protecting this finite number
111 of cells is, therefore, an important therapeutic goal [10].

112 Lately, first studies have indicated the importance of genome maintenance for renal health [11,12].
113 Mutations in the kinase endopeptidase and other proteins of small size (KEOPS) complex genes
114 caused proteinuria and induced DNA damage response (DDR) *in vitro* [13]. Likewise, glomerular
115 DNA damage was found to be associated with declining kidney function [14] and cells isolated from
116 the urine of patients suffering from diabetes and hypertension showed increased levels of DNA
117 strand breaks [15]. First evidence of nucleotide excision repair (NER) being an essential pathway in
118 kidney health was recently provided through the identification of *ERCC1* variants causing kidney
119 dysfunction in patients [16]. However, this study mostly reported on a tubulopathy phenotype, hence,
120 the link between DNA damage and podocyte loss remains unclear.

121 Several studies have proposed an interplay between DNA damage signaling and the mechanistic
122 target of rapamycin (mTOR) pathway with factors induced by DNA damage exhibiting repressive
123 effects on mTOR-complex1 (mTORC1) [17–19] and increased mTORC1 activity leading to genomic
124 stress [20–22]. This is of particular interest for podocytes, as they are highly dependent on a rigorous
125 control of mTOR activity. While mTORC1-driven hypertrophy is a protective response upon
126 podocyte depletion [23–25], mTORC1 overactivation drives pathologic hyperproliferation and
127 sclerosis [26,27]. In line with these findings, side effects of pharmacological mTORC1 inhibition entail
128 proteinuria and glomerular scarring [28–34].

129 In this study, we identified perturbations in the expression of DNA repair genes in glomeruli from
130 various human glomerular diseases associated with podocyte depletion and a significant loss of
131 NER gene expression in podocytes of FSGS patients. Podocyte-specific DNA damage

132 accumulation through NER disruption resulted in proteinuria, podocyte loss, glomerulosclerosis,
133 and renal insufficiency in mice. Ancillary, DNA damage accumulation was identified as a hallmark
134 of murine and human podocyte aging. Strikingly, both *in vivo* and *in vitro* analyses revealed
135 mTORC1 activation upon DNA damage, indicating a cell-type specific response. Inhibiting parts
136 of the DNA damage response diminished mTORC1 activation and, in turn, inhibiting mTORC1
137 activation ameliorated glomerulosclerotic phenotypes in two NER-deficient mouse models. These
138 results directly link genome maintenance to mTORC1 signaling and glomerular diseases.
139
140 **Methods:**
141 *ERCB Human microarray analysis*
142 167 genes involved in DNA repair and nucleotide excision repair were compiled from the hallmark
143 gene set "DNA-Repair" from the Molecular Signatures Database (MSigDB) Collection[35] and upon
144 literature research. Human kidney biopsies and Affymetrix microarray expression data were
145 obtained within the framework of the European Renal cDNA Bank - Kröner-Fresenius Biopsy Bank
146 [36]. Diagnostic biopsies were obtained from patients after informed consent and with approval of
147 the local ethics committees. Following renal biopsy, the tissue was transferred to RNase inhibitor
148 and micro-dissected into glomeruli and tubulo-interstitium. Total RNA was isolated, reverse
149 transcribed, and amplified to a protocol previously reported [37]. Fragmentation, hybridization,
150 staining, and imaging were performed according to the Affymetrix Expression Analysis Technical
151 Manual (Affymetrix, Santa Clara, CA, USA). Published datasets of glomerular samples were
152 analysed for mRNA expression levels. Analysis included datasets from patients with minimal
153 change disease (MCD; n=14), focal segmental glomerulosclerosis (FSGS; n=23), membranous
154 nephropathy (MGN; n=21), IgA nephropathy (Glom; n=27), and hypertensive nephropathy (HTN;
155 n=15) as well as controls (living donors (LD); n=42) (GSE99340, LD data from: GSE32591,
156 GSE37463). CEL file normalization was performed with the Robust Multichip Average method
157 using RMAExpress (Version 1.0.5) and the human Entrez-Gene custom CDF annotation from
158 Brain Array version 18 (http://brainarray.mbni.med.umich.edu/Brainarray/default.asp). To identify
159 differentially expressed genes, the SAM (Significance Analysis of Microarrays) method [38] was
160 applied using SAM function in Multiple Experiment Viewer (TiGR MeV, Version 4.9). A q-value
161 below 5% was considered to be statistically significant. The resulting gene expression list was
162 censored for genes, whose products were detected in a transcriptomic and proteomic analysis of
163 wild-type murine podocytes [39].
164 *Single nucleus sequencing*

165 Nuclei were prepared from kidney biopsy cores stored in RNAlater from FSGS patients enrolled
166 in the NEPTUNE study. The processing followed the protocol developed from the Kidney Precision
167 Medicine Project. Nuclei preparations were processed and sequenced using 10x Genomics single
168 cell sequencer. Analyses were performed on the output data files from CellRanger v6.0.0 using
169 the Seurat R package (version 3.2 and 4.0; https://cran.r-
170 project.org/web/packages/Seurat/index.html). To limit low quality nuclei and/or multiplets, we set
171 gene counts and cutoffs to between 500 and 5000 genes and examined nuclei with a mitochondrial
172 gene content of less than 10%. Nuclei were merged into a Seurat object using the CCA integrate
173 function and nuclear cluster annotation was determined by finding enriched genes in each cell
174 cluster. A comparison of these cluster selective gene profiles was compared against previously
175 identified cell marker gene sets from human kidney samples from KPMP and other sources [40].
176 *Mice*
177 Mice were bred in a mixed FVB/CD1 (*Ercc1* pko) or FVB/CD1/C57BL6 (*Ercc1* ipko) background.
178 All offspring was born in normal mendelian ratios. Mice were housed in the animal facility of the
179 Center for Molecular Medicine Cologne or the Cluster of Excellence – Cellular Stress Responses
180 in Aging-Associated Diseases. Following federal regulations, the Animal Care Committee of the
181 University of Cologne reviewed and approved the experimental protocols. Animals were housed
182 at specific pathogen-free (SPF) conditions with three-monthly monitoring according to FELASA
183 suggestions. Housing was done in groups of less than six adult animals receiving CRM pelleted
184 breeder and maintenance diet irradiated with 25 kGy (Special Diet Services, Witham, UK) and
185 water *ad libitum*. Spot urine was collected once a week during cage changes or during sacrifice.
186 Tamoxifen was administered at 400 mg/kg Tamoxifen in dry chow.
187 For rapamycin injection studies male and female *Ercc1*$^{fl/fl}$ (ctrl) and *Ercc1*; *pod-cre* (pko) mice at
188 week 6 of age were injected intraperitoneally 3 times/week with 2 mg/kg bw of rapamycin diluted
189 in 5% ethanol, 5% tween 80 and 5% PEG 400 or with 5% ethanol, 5% tween 80 and 5% PEG 400
190 as vehicle. Urine collection was performed 2 times/week and mice were sacrificed at week 13 of
191 age for serum and kidney tissue isolation. All animals were maintained in grouped cages on a 12h
192 light/dark cycle. Mice were kept on a regular diet and had access to water *ad libitum*. Body weight
193 was measured weekly. Animals were housed in a temperature-controlled, pathogen-free animal
194 facility at the Institute of Molecular Biology and Biotechnology (IMBB), which operates in
195 compliance with the "Animal Welfare Act" of the Greek government, using the "Guide for the Care
196 and Use of Laboratory Animals" as its standard.
197 Mice were anaesthetized by intraperitoneal injection of 10 μl per g bodyweight of 0,01% xylocaine

198 and 12,5 mg/ml ketamine – blood was drawn from the left ventricle into a syringe rinsed with
199 Heparin sulfate, and animals were perfused with cold phosphate buffered saline (PBS). Kidneys
200 were excised and embedded in OCT (Sakura, Torrance, CA) and frozen at -80°C or fixed in 4%
201 neutral buffered formalin and subsequently embedded in paraffin.

202 *Podocyte isolation*

203 To isolate primary podocytes, *Ercc1*$^{fl/fl}$ mice heterozygous for the *R26mTmG* and *NPHS2.Cre*
204 transgene were sacrificed and kidneys were used for glomerular preparation, as previously
205 described [39]. The glomeruli were digested and the single-cell suspension was used for
206 fluorescence-activated cell sorting.

207 *qPCR Analysis*

208 Total ribonucleic acid (RNA) was extracted from podocytes of *Ercc1/Pod:Cre/mTmG* mice using
209 Direct-zol™ RNA MiniPrep Kit (cat. no. R2052, Zymo Research). Isolation of glomeruli,
210 preparation of a glomerular single-cell suspension, and fluorescence-activated cell sorting was
211 done as previously described [7]. Podocytes were sorted into TriReagent (cat. no. 93289, Sigma-
212 Aldrich). The complementary deoxyribonucleic acid (cDNA) was synthesized with High Capacity
213 cDNA Reverse Transcription Kit (cat. no. 4368814, Applied Biosystems). PCR was performed
214 using TaqMan™ Gene Expression Master Mix (cat. no. 4369016, Applied Biosystems) and the
215 Applied Biosystems Real-time PCR system. Real-time PCR was measured with triplicates in each
216 gene target. The sequence of the PCR primer used for *Ercc1* was: 5′-
217 AGCCAGACCCTGAAAACAG-3′ and 5′- CACCTCACCGAATTCCCA-3′ in PrimeTime Mini qPCR
218 Assay for *Ercc1* (Assay-ID: Mm.PT.58.42152282, IDT). The gene expression was calculated using
219 comparative cycle threshold method and normalized to RNA polymerase II subunit A (*Polr2a*).
220 The relative fold change of *Ercc1* expression in knockout mice was compared with WT and
221 heterozygous mice.

222 *Urinary Albumin ELISA & Creatinine measurement*

223 Urinary albumin levels were measured with a mouse albumin ELISA kit (mouse albumin ELISA
224 kit; Bethyl Labs, Montgomery, TX, USA). Urinary creatinine kit (Cayman Chemical, Ann Arbor, MI,
225 USA) was used to determine corresponding urinary creatinine values. For Coomassie Blue
226 detection of albuminuria, spot urine of mice was diluted 1:20 in 1x Laemmli buffer and urinary
227 proteins separated using poly-acrylamide gel electrophoresis with subsequent Coomassie gel
228 stain.

229 *Plasma Creatinine and Urea measurement*

230 Blood samples were centrifuged at 400 g 4°C for 20 minutes and plasma samples subsequently
231 stored at -20°C until further analysis. Creatinine and Urea were measured using standard clinical
232 protocols by the Department of Clinical Chemistry of the University of Cologne.

233 *Histologic analysis*

234 To assess morphological changes in light microscopy we performed Periodic Acid Schiff staining.
235 For specific antibody stainings sections were deparaffinized in Xylene (VWR, Darmstadt,
236 Germany), rehydrated in decreasing concentrations of ethanol, and subjected to heat-induced
237 antigen retrieval in 10 mM Citrate Buffer pH 6 for 15 minutes. Peroxidase blocking was performed
238 in methanol mixed with 3% hydrogen peroxidase (Roth, Karlsruhe, Germany) followed by
239 Avidin/Biotin Blocking (Vector, Burlingame, CA, USA) for 15 minutes each. After incubation in
240 primary antibody (anti-phospho-S6 Ribosomal Protein (Ser235/236) # 4858 – Cell Signaling
241 Technology) 1:200 in TBS 1% BSA at 4°C overnight, sections were washed in TBS and incubated
242 in biotinylated secondary antibody (Jackson Immunoresearch, West Grove, USA) 1h at room
243 temperature. For signal amplification the ABC Kit (Vector, Burlingame, CA, USA) was used before
244 applying 3,30-diaminobenzamidine (Sigma-Aldrich, St Louis, USA) as a chromogen. Hematoxylin
245 was used for counterstaining. After dehydration, slides were covered in Histomount (National
246 Diagnostics, Atlanta, USA).

247 *Immunofluorescence Staining*

248 Paraffin embedded tissue was cut into 3 μm thick sections and processed according to published
249 protocols [41]. Primary antibodies (anti-γH2A.X #2577s – Cell Signalling Technology, anti-nephrin
250 #GP-N2 – Progen, anti-synaptopodin #65294 – Progen, anti-Dach1 #HPA012672 – Sigma Aldrich
251 [42], anti-phospho-S6 Ribosomal Protein (Ser235/236) # 4858 – Cell Signaling Technology), and
252 anti-p53 (anti-p53 #p53-protein-cm5 Leica Biosystems) were used at 1:200 dilution. Far-red
253 fluorescent DNA dye Draq 5 was used as a nuclear marker.

254 Cells were processed according to published protocols [43].

255 For γH2A.X foci quantification, a custom-built FIJI macro was used. In brief, podocyte nuclei were
256 identified through surrounding synaptopodin staining, segmented using the freehand tool and split
257 into single channels. Draq 5 channel was converted into binary image using auto threshold "otsu
258 dark" with subsequent particle measurement (range 5-Infinite) to determine nuclear area. γH2A.X
259 channel was converted into binary image using auto threshold "MaxEntropy dark" with subsequent
260 particle measurement (range 0.02-infinite) to determine foci number and area.

261 *Electron Microscopy*

262 Mice were perfused with 4% paraformaldehyde and 2% glutaraldehyde in 0.1 M sodium
263 cacodylate, pH 7.4. Postfixation was performed in the same buffer for two additional weeks at 4°C.
264 Tissue was osmicated with 1% OsO4 in 0.1 M cacodylate and dehydrated in increasing ethanol
265 concentrations. Epon infiltration and flat embedding were performed following standard
266 procedures. Toluidine blue was used to stain semithin sections of 0.5 μm. 30 nm-thick sections
267 were cut with an Ultracut UCT ultramicrotome (Reichert) and stained with 1% aqueous uranylic
268 acetate and lead citrate. Samples were studied with Zeiss EM 902 and Zeiss EM 109 electron
269 microscopes (Zeiss, Oberkochen, Germany).

270 *In vitro Experiments*

271 Conditional immortalized murine podocytes were a gift by Stuart Shankland. Cells were cultured
272 as previously described [44]. Briefly, immortalized podocytes were cultured in RPMI media
273 supplemented with 10% FBS and IFNγ (Sigma-Aldrich, Taufkirchen, Germany). Cells proliferated
274 at 33°C on Primaria plastic plates (BD Biosciences, San Jose, CA, USA) until they reached a
275 confluence of 60-70%. Differentiation of podocytes was induced by seeding the cells at 37°C in
276 the absence of IFNy. After 10 days of differentiation, cells were treated with 5 or10 μg/ml
277 Mitomycin C (#M0503 - Sigma-Aldrich, Taufkirchen, Germany) for 2h in serum-free medium,
278 followed by one washing step with Phosphate-Buffered Saline and further incubation for 6 h in
279 serum-free medium without Mitomycin C before further processing. The absence of mycoplasm
280 infection was tested regularly using the mycoplasm detection kit from Minerva biolabs (Minerva
281 Biolabs, Berlin, Germany). For experiments with DNA damage response inhibitors, differentiated
282 cells were pre-treated with 3 μM KU60019 (Selleckchem, Houston, TX, USA) or 1 μM Nedisertib
283 (Selleckchem, Houston, TX, USA) for 1 h before inducing DNA damage by UV-C or Mitomycin C
284 treatment. Inhibitors were added again after medium change following DNA damage induction to
285 further incubate cells for 6 h before cell lysis.

286 *Western Blot analysis*

287 SDS-PAGE was used for protein size separation with subsequent blotting onto polyvinylidene
288 difluoride membranes and visualized with enhanced chemiluminescence after incubation of the
289 blots with corresponding antibodies (Phospho-Histone H2A.X (Ser139); Phospho-S6 Ribosomal
290 Protein (Ser235/236) (D57.2.2E); S6 Ribosomal Protein (5G10) – Cell Signaling Technology;
291 alpha Actin – Developmental Studies Hybridoma Bank; beta-Tubulin (E7) - Developmental Studies
292 Hybridoma Bank).

293 *eQTL Analysis*

294 For the subgroup analysis of FSGS cohort, the procedure described in Gillies et al., 2018 was
295 used with the following exceptions: only FSGS patients were analysed (N=87) and only RNAseq
296 expression data for glomerular samples were utilized. Briefly cis-eQTLs were identified using
297 MatrixEQTL from among variants that were located either within the annotated boundaries of a
298 gene or its surrounding region (+/- 500 kb) [45]. We then adjusted for age, sex, principal components
299 of genetic ancestry, and the first 5 PEER factors [46]. The genetic ancestry was calculated using
300 LD-pruned WGS data from across all 87 patients using the EPACTS tool
301 (https://genome.sph.umich.edu/wiki/EPACTS). The gene-level FDR for the MatrixEQTL was
302 controlled using TORUS. Fine mapping of the eQTLs was performed using the DAP algorithm [47].
303 *Study approval*
304 All investigations involving human specimen have been conducted according to the Declaration
305 of Helsinki following approval of the local ethics committees. Written informed consent was
306 received from participants prior to inclusion in the study. All mouse experiments were conducted
307 according to institutional and federal guidelines and approved by the LANUV NRW VSG 84-
308 02.04.2013.A336.
309 *Statistics*
310 If not stated otherwise, unpaired two tailed Student's t-test was used to compare two groups and
311 p values ≤ 0.05 were considered significant. For multiple group comparisons, we applied 1-way
312 ANOVA followed by Tukey's post hoc correction. Statistics were performed using GraphPad Prism
313 8.
314
315 **Results:**
316 **DNA damage repair is essential for podocyte health and is impaired in focal segmental**
317 **glomerulosclerosis**
318 To determine the involvement of the NER pathway in podocyte loss, we investigated the
319 expression of NER genes in podocytes of FSGS biopsies, Minimal change disease (MCD) patients
320 and controls using single nucleus sequencing. Indeed, we detected an upregulation in the *Ercc1*-
321 8 genes, all involved in damage recognition, DNA unwinding and damage excision, in FSGS
322 podocytes when compared to MCD and living donor kidney samples (Fig. 1A). Conversely the
323 expression of various polymerases involved in the synthesis of new repaired strands was virtually
324 lost in the podocytes of both MCD and FSGS samples indicative of a predominance of damage
325 recognition and strand excision in the FSGS biopsies (Fig. S1A). Targets of the mTORC1

326 pathway, used as an internal control, increased in expression with little changes in the percentage
327 of podocytes expressing these genes (Fig. S1A).
328 Likewise, we detected a wide array of alterations in the expression of DNA repair and NER genes
329 in glomerular lysates of different nephropathies compared to controls (Fig. S1B; Tbl. S1)
330 Furthermore, we assessed whether genetic variants associated with glomerular mRNA expression
331 of DNA repair genes could be detected in patients with sclerotic glomerular diseases (Table S2)
332 and we identified single nucleotide polymorphisms (SNPs) associated with alterations in the
333 expression of DNA repair genes (Table S2 - S4).
334 As the perturbation of NER genes in FSGS podocytes could indicate defective DNA repair
335 mechanisms, we investigated the accumulation of DNA damage in podocyte nuclei using γH2A.X
336 immunofluorescence staining in human biopsies of FSGS compared to MCD patients. Indeed, we
337 detected a marked increase in podocyte-specific nuclear γH2A.X foci in FSGS glomeruli (Fig. 1B
338 & S1C, D & E), corresponding to DNA double-strand breaks and thus suggestive of an involvement
339 of DNA damage accumulation in podocyte damage and loss.
340 A well-established model to induce DNA damage *in vivo* is to induce a functional impairment of
341 the NER cascade by deletion of the endonuclease Ercc4's co-factor, the DNA excision repair
342 protein Ercc1 [48–50]. Investigating glomeruli of the *Ercc1* -/delta mouse [51], a mouse model with whole
343 body disruption of *Ercc1* on one allele and a truncated form of *Ercc1* on the second allele, leading
344 to a hypomorphic variant with minimal residual activity, already revealed the development of foot
345 process effacement at 14 weeks of age (Fig. S2A).
346 These findings pointed towards DNA damage repair as an essential mechanism for podocyte
347 health. Thus, we generated a constitutive podocyte-specific knockout of *Ercc1* using the cre-loxP
348 system in mice of mixed FVB/CD1 background [52] (Fig. S2B & 1C.). Mice carrying the podocyte-
349 specific knockout (pko) had a decreased lifespan of 10-15 weeks, while cre negative animals (ctrl)
350 and cre positive animals heterozygous for the floxed *Ercc1* allele (het) were investigated for up to
351 72 weeks without overt abnormalities (Fig. 1D & S2C & D). While weight gain after birth was
352 normal up to week 9, *Ercc1* pko offspring displayed a pronounced decrease of weight thereafter
353 (Fig. 1E). This weight drop was accompanied by the development of significant albuminuria as
354 well as elevated serum creatinine and urea levels, starting at week 11 (Fig. 1F-H). At week 13,
355 *Ercc1* pko mice had developed severe generalized renal damage, including glomerulosclerosis,
356 interstitial fibrosis, and tubular atrophy with protein casts (Fig. 1I).
357 Similar results could be obtained in a tamoxifen-inducible podocyte specific knockout (ipko) of
358 *Ercc1* (Fig. S3).

359

360 **DNA damage accumulation in podocytes triggers cellular stress and podocyte loss**

361 Ultrastructural alterations in 9-week-old constitutive *Ercc1* pko glomeruli were detectable in the
362 form of focally effaced podocyte foot processes. These changes were not yet present in 7-week-
363 old animals (Fig. 2A). Further evidence of podocyte stress was revealed by gradual reduction of
364 nephrin expression, an important slit diaphragm protein, from weeks 9 to 13 (Fig. 2B & S4A).
365 Podocyte number, glomerular hypertrophy, and podocyte density, investigated through staining of
366 the podocyte specific proteins synaptopodin (SNP) and Dachshund Family Transcription Factor 1
367 (Dach1) remained within normal ranges at week 9 (Fig. 2C & S4B). In contrast, glomeruli from 11-
368 week-old *Ercc1* pko mice clearly showed severe injury and loss of podocytes, indicated by the
369 decrease and loss of both SNP and Dach1 (Fig. 2D). This loss of podocytes was further validated
370 through the analysis of WT1-positive cells in 9- and 11-week-old *Ercc1* pko mice (Fig. S4C).
371 Foci of phosphorylated histone 2A.X (γH2A.X), a *bona fide* marker for DNA double-strand breaks,
372 were significantly increased in both number and area in podocyte nuclei of *Ercc1* pko glomeruli at
373 week 9 (Fig. 2E & S4D-F) compared to control animals. Strikingly, we also observed a smaller
374 number of γH2A.X foci in almost all wildtype podocyte nuclei indicative of constant DNA damage
375 occurrence and subsequent repair in healthy glomeruli. At later time points, single podocytes with
376 γH2A.X signals covering larger areas of the nuclei became apparent in *Ercc1* pko glomeruli (Fig.
377 2F).

378

379 **DNA damage accumulation in podocytes activates the mTORC1 pathway *in vivo***

380 Podocyte loss is tightly linked to mTORC1 activation and cellular hypertrophy of the remaining
381 podocytes. Therefore, we investigated the timepoint of mTORC1 activation in *Ercc1* pko mice.
382 Strikingly, we detected a significant increase in pS6RP-positive cells in *Ercc1* pko glomeruli at 9
383 weeks of age (Fig. 3A), a timepoint, when no evidence for podocyte loss was present yet (Fig. 2C
384 & S4C). In-detail analysis revealed that more than 40% of podocytes showed mTORC1 activation
385 at week 9 (Fig. 3A).
386 To investigate whether increased mTORC1 signaling contributes to the development of podocyte
387 loss, we analysed the kidneys of *Ercc1* -/delta mice treated with 14 mg/kg food of the mTORC1
388 inhibitor rapamycin from 8 weeks of age until termination of the experiment due to high moribund
389 scoring [53]. Despite the fact that the treated cohort did not present with an extended lifespan,
390 moribund animals of the end-of-life cohort (aged 15-26 weeks) presented with a significant
391 reduction of sclerotic glomeruli, when treated with rapamycin (Fig. 3B). Additionally, we treated

392 our podocyte-specific *Ercc1* ko mouse model with 2 mg/kg bodyweight rapamycin via i.p. injections
393 three times a week, beginning at 6 weeks of age. Again, we detected a significant reduction in
394 globally sclerotic glomeruli and more healthy glomeruli upon rapamycin treatment at the end of
395 our observation period at week 13 (Fig. 3C).
396 The observed detection of increased mTORC1 signaling and DNA damage accumulation
397 suggests a potential interplay. It has been suggested that increased mTORC1 signaling decreases
398 the cellular ability to repair DNA damage [20,21]. Thus, we investigated the occurrence of γH2A.X
399 foci accumulation in a podocyte-specific *Tsc1* knockout mouse model characterized by podocyte-
400 specific mTORC1 hyperactivation [25,54]. Indeed, *Tsc1* pko mice also depicted an increased number
401 of DNA damage foci as early as 4 weeks of age, when the phenotype is predominantly driven by
402 mTORC1 hyperactivation (Fig. 3D).
403 This data indicates increased mTORC1 signaling through DNA damage accumulation and
404 decreased DNA damage repair upon mTORC1 activation potentially constituting a downward
405 spiral aggravating podocyte damage (Fig. 3E).
406
407 **DNA damage activates the mTORC1 cascade through DNA damage signaling kinase DNA-**
408 **PK in podocytes**
409 To further investigate the mechanism behind mTORC1 activation occurring in podocytes upon
410 genomic stress, we induced DNA damage through mitomycin C (MMC) treatment and UV-C
411 irradiation *in vitro* in immortalized mouse podocytes (Fig. 4A). These treatments led to significant
412 increases of γH2A.X (Fig. 4B) and accumulation of the DNA damage response protein p53 in the
413 nucleus (Fig. 4C). Again, DNA damage induced an increased phosphorylation of S6 ribosomal
414 protein (pS6RP), which is a downstream target of mTORC1, in podocytes (Fig. 4D). This
415 phosphorylation was completely abrogated by mTORC1 inhibitor rapamycin and reduced by
416 serum starvation, a well-known mTORC1 modulator[55]. In order to identify the link between DNA
417 damage accumulation and mTORC1 activation, we treated MMC- or UV-C-stimulated murine
418 podocytes with inhibitors of the DNA damage signaling cascade (Fig. 4E). In both conditions,
419 inhibition of DNA-dependent protein kinase (DNA-PK) by Nedisertib resulted in abrogation of
420 S6RP phosphorylation. Similar results could be achieved with the Ataxia Telangiectasia Mutated
421 serine/threonine kinase (ATM) inhibitor KU60019. No effects were detected upon treatment with
422 the ATR inhibitor VE822 or with the CHK1 inhibitor prexasertib (data not shown). These data
423 indicate a direct mechanistic link between genomic stress and mTORC1 signaling in podocytes.

424 Since genomic stress represents a hallmark of cellular aging, we investigated both murine and
425 human glomeruli of young and aged subjects. Indeed, the well-documented increase in mTORC1
426 signaling in aged murine podocytes coincided with increased detection of DNA damage foci (Fig.
427 4F & S5A). Similar results were detected in a series of human tumor nephrectomy samples when
428 comparing a young group (21-49 years; n=4) with an old group (69-81 years; n=5) (Fig.4G & S5B).
429 These results validate the occurrence of DNA damage in both healthy murine and human
430 podocytes and indicate an association between DNA damage and aging in podocytes, possibly
431 contributing to age-related podocyte loss [25].
432
433 **Discussion**:
434 Our study allows two principal conclusions: (1) DNA repair mechanisms are involved in the
435 pathophysiology of glomerular disease, which are indispensable for podocyte homeostasis, and
436 (2) podocytes respond to DNA damage by upregulation of the mTORC1 pathway in a DNA-PK-
437 mediated manner before the onset of podocyte loss, not via a repression of the mTORC1 pathway.
438 Together, this is the first report drawing a connection between DNA repair mechanisms and
439 glomerular diseases via mTORC1 signaling.
440 Only recently the importance of DNA repair has sparked larger interest in the field of podocyte
441 biology. Due to their often deleterious clinical phenotypes in humans, the description of glomerular
442 abnormalities in syndromes caused by mutations in DNA repair genes is scarce [56,57]. However,
443 there is evidence for podocyte involvement in syndromes caused by mutations of DNA repair
444 genes underlined by reports of patients exhibiting proteinuria and nephrotic syndrome [49,58,59]. The
445 same holds true for factors involved in other forms of DNA maintenance such as the KEOPS
446 complex [13,60] or KAT5, a contributor to DNA methylation and non-homologous endjoining repair [61].
447 Itoh and co-workers linked proteinuric kidney diseases due to hypertension and diabetes to DNA
448 double-strand breaks and methylation in the promotor region of the slit diaphragm protein nephrin
449 and established an association to DNA double-strand breaks in glomeruli of patients suffering from
450 IgA nephropathy [14,15]. Our analysis adds considerably to this body of evidence, as we identify
451 multiple factors of DNA maintenance, in particular of NER, to be transcriptionally altered in
452 glomeruli of different renal diseases involving pronounced podocyte damage and loss. This is in
453 line with decreased expression of NER endonuclease ERCC4 in IgA nephropathy[14]. The precise
454 evaluation of perturbations in every single one of the identified genes goes beyond the scope of
455 this manuscript, but we delineated the striking decrease of NER gene expression in FSGS

456 podocytes and investigated the podocyte-specific reaction to accumulating DNA damage in depth
457 *in vivo* and *in vitro*.
458 To what extent glomerular epithelial cells are subjected to genomic stress is currently unclear. For
459 the first time, this study reveals the occurrence of individual DNA damage foci in podocytes under
460 healthy conditions indicating a need for constant DNA maintenance and repair in this specialized
461 cell type. This finding is in line with studies investigating glomerular expression profiles of a partial
462 *Ercc1* knockout [62] and an adipose tissue-specific *Ercc1* knockout that described a low amount of
463 DNA damage foci also occurring in adipocytes of control animals [50]. A major factor contributing to
464 this stress may result from damaging agents in the serum, as serum components are constantly
465 filtered into the primary urine in which the podocytes are emerged in. Since podocytes entail very
466 little capacity for regeneration [7], they are in specific need for efficient repair of occurring DNA
467 damage and particularly vulnerable to abrogation of these repair pathways. Deficiency in the repair
468 of DNA damage seems to be compensable up to a certain threshold as podocyte loss, proteinuria,
469 and glomerular sclerosis only became apparent after week 9 in our mouse model. In line with
470 these findings, decreased *Ercc1* gene expression in heterozygous mice appears to be sufficient
471 to maintain healthy glomeruli, as these animals depict no phenotype at one year of age. Yet, the
472 presence of foot process effacement and glomerulosclerosis in *Ercc1* -/delta mice indicates that
473 minimal residual activity is not sufficient for podocyte health.
474 The interplay of DNA damage, its repair, and the mTOR pathway has been a subject of numerous
475 studies, specifically in the field of cancer biology. These studies indicated that mTORC1 signaling
476 is inhibited upon DNA damage in a TSC, Sestrin or AKT dependent manner [17,18,19]. Strikingly, we
477 observed that podocytes both *in vitro* and *in vivo* reacted to endogenous accumulation or
478 exogenous infliction of DNA damage with activation of the mTORC1 pathway. Herein lies a
479 fundamental difference to past reports and a potential disease mechanism as numerous studies
480 have depicted the importance of a tight regulation of mTORC1 for podocyte health and the
481 deleterious effects of both overactivation and repression in disease [23,25,26,43,63,64]. Since mTORC1
482 activation occurs in *Ercc1* pko podocytes at 9 weeks, a time point of no overt podocyte loss, mild
483 ultrastructural differences, and significant accumulation of DNA damage foci, our data indicate a
484 direct link between genomic stress and mTORC1 activation in podocytes via activation of DNA-
485 PK.
486 A growing body of evidence suggests that mTORC1 activity reduces the capacity of successful
487 DNA repair [20,21], e.g. through ribosomal S6 kinase (S6K)-dependent phosphorylation of E3
488 ubiquitin-protein ligase RNF168 [22]. However, upon podocyte depletion, remaining podocytes on

489 the glomerular tuft counteract the loss of neighbouring cells through mTORC1-mediated
490 hypertrophy [25] which impairs proper DNA repair. This fact is underlined by podocyte-specific *Tsc1*
491 knockout animals displaying mTORC1 hyperactivation, which accumulate a significantly increased
492 amount of DNA damage foci already at 4 weeks of age. We, therefore, hypothesize that this
493 reaction can lead to a downward spiral of insufficient DNA maintenance further aggravated
494 through mTORC1 activation and, despite of mTORC1 mediated hypertrophy, trigger excessive
495 podocyte loss. This cascade could potentially be ameliorated through well-timed mTORC1
496 inhibition as indicated by the reduction of glomerulosclerosis in rapamycin-treated *Ercc1* -/delta
497 and *Ercc1* pko animals or upregulation of DNA repair mechanisms to alleviate accumulated
498 genomic stress. Potential sites in the genome that could be used to alter glomerular damage repair
499 were already identified in our eQTL analysis in FSGS patients. This is of particular interest since
500 there seems to be a broad interplay between gene products exerting functions beyond their
501 canonical pathways in genome maintenance [65]. Likewise, decreased expression of DNA repair
502 genes in a subset of patients or the accumulation of DNA damage through the aging process may
503 lead to increased mTORC1 activation in podocytes, thereby rendering a subgroup of patients
504 vulnerable to the development of glomerular disease and scarring.
505 The importance of DNA damage repair in podocyte homeostasis is consistent with the role in other
506 postmitotic cell types and particularly apparent in neurodegenerative pathologies typical for NER
507 deficiency syndromes [5]. The role of NER in repairing transcription-blocking lesions might thus play
508 a pivotal role in podocytes that need to maintain the integrity of transcribed genes during the entire
509 lifespan of the organism. Even hepatocytes of *Ercc1* -/delta mice, usually characterized by high
510 self-renewing potential, showed a considerable block of transcription, indicative of transcription-
511 coupled mechanisms being stalled [66,47].
512 In conclusion, we identified nucleotide excision repair as an essential mechanism of DNA
513 maintenance in podocyte homeostasis. The presented study characterizes the activation of
514 mTORC1 signaling as a podocyte-specific response to DNA damage and identifies the
515 accumulation of DNA damage as one novel hallmark of podocyte loss and glomerular disease,
516 suitable for precision medicine approaches.
517
518 **Disclosures:**
519 The authors declare no conflict of interest.
520

Author contributions:

FB, AMM, LB, RAH, VGP, MNW, GC, MR, DF, GGS, SK, MTL, WB, VN, PM performed experiments; FB, LB, AMM, GC, RAH, VGP, MNW, DF, MTL, WB, MGS, VN analysed data; FB, AMM, VGP, GG, MD, PTB, CDC, MK, MGS, MK, TBH, BSche, TB, BSchu, CEK conceived experiments, FB, VGP, BSchu, CEK wrote the manuscript, all authors revised the manuscript, all authors agreed on the publication in the presented state.

Funding:

Fabian Braun received funding from the Else-Kröner-Fresenius-Stiftung: Else-Kröner-Memorial Stipendium / 2021_EKMS.26

Amrei M. Mandel was partially funded by the Else Kröner-Fresenius-Stiftung and the Eva Luise und Horst Köhler Stiftung – Project No: 2019_KollegSE.04.

Linda Blomberg was supported by the Faculty of Medicine, of University of Cologne: Koeln Fortune Program KF 12/2020.

Victor Puelles received support from the Deutsche Forschungsgemeinschaft: Clinical Research Unit / CRC1192, and the Bundesministerium für Bildung und Forschung eMed Consortia / Fibromap) and the Novo Nordisk Foundation (NNF21OC0066381).

Georgia Chatzinikolaou is supported by ELIDEK grant agreement No 1059, funded from the Hellenic Foundation for Research and Innovation (HFRI) and the General Secretariat for Research and Technology (GSRT).

Gisela G. Slaats was supported by an EMBO long-term fellowship ALTF 475-2016 and the Fritz Thyssen Foundation project 10.20.1.012MN.

Martijn Dollé received support the National Institute of Health (NIH)/National Institute of Aging (NIA) (AG17242)

Paul T. Brinkoetter received support from the Deutsche Forschungsgemeinschaft: Clinical research unit: KFO 329, BR 2955/8-1, and the Bundesministerium für Bildung und Forschung STOP-FSGS 01GM1901E

Matthew G. Samspon is supported by NIH grants RO1 DK108805, DK119380, and RC2 DK122397

George A. Garinis was supported by ELIDEK grant 631, funded from the Hellenic Foundation for Research and Innovation (HFRI).

The George M. O'Brien Michigan Kidney Translational Core Center was funded by NIH/NIDDK grant 2P30-DK-081943.

554 Bernhard Schermer received support by the Deutsche Forschungsgemeinschaft: Clinical research
555 unit KFO 329 SCHE 1562/7-1.
556 Thomas Benzing received support from the Deutsche Forschungsgemeinschaft: Clinical research
557 unit: KFO 329, BE 2212/23-1 & 2212/24-1, and the Bundesministerium für Bildung und Forschung
558 STOP-FSGS 01GM1901E
559 Christine Kurschat received support by the Deutsche Forschungsgemeinschaft: Clinical research
560 unit KFO 329 KU 1539/5-1.
561
562 **References:**
563
564 1. Lindahl T, Nyberg B: Rate of depurination of native deoxyribonucleic acid. *Biochemistry-us* 11:
565 3610–3618, 1972
566 2. Loeb LA, Harris CC: Advances in chemical carcinogenesis: a historical review and
567 prospective. *Cancer Res* 68: 6863–72, 2008
568 3. Chatterjee N, Walker GC: Mechanisms of DNA damage, repair, and mutagenesis: DNA
569 Damage and Repair. *Environ Mol Mutagen* 58: 235–263, 2017
570 4. Ghosal G, Chen J: DNA damage tolerance: a double-edged sword guarding the genome.
571 *Transl Cancer Res* 2: 107–129, 2013
572 5. Wolters S, Schumacher B: Genome maintenance and transcription integrity in aging and
573 disease. *Frontiers Genetics* 4: 19, 2013
574 6. Madabhushi R, Pan L, Tsai L-H: DNA damage and its links to neurodegeneration. *Neuron* 83:
575 266–82, 2014
576 7. Wanner N, Hartleben B, Herbach N, Goedel M, Stickel N, Zeiser R, et al.: Unraveling the role
577 of podocyte turnover in glomerular aging and injury. *Journal of the American Society of*
578 *Nephrology : JASN* 25: 707–716, 2014
579 8. Butt L, Unnersjö-Jess D, Höhne M, Edwards A, Binz-Lotter J, Reilly D, et al.: A molecular
580 mechanism explaining albuminuria in kidney disease. *Nat Metabolism* 2: 461–474, 2020
581 9. Chen TK, Knicely DH, Grams ME: Chronic Kidney Disease Diagnosis and Management.
582 *Jama* 322: 1294–1304, 2019
583 10. Rosenberg AZ, Kopp JB: Focal Segmental Glomerulosclerosis. *Clinical journal of the*
584 *American Society of Nephrology : CJASN* 12: 502–517, 2017
585 11. Marshall CB, Pippin JW, Krofft RD, Shankland SJ: Puromycin aminonucleoside induces
586 oxidant-dependent DNA damage in podocytes in vitro and in vivo. *Kidney Int* 70: 1962–1973,
587 2006
588 12. Hakroush S, Cebulla A, Schaldecker T, Behr D, Mundel P, Weins A: Extensive Podocyte
589 Loss Triggers a Rapid Parietal Epithelial Cell Response. *Journal of the American Society of*
590 *Nephrology : JASN* 25: 927–938, 2014
591 13. Braun DA, Rao J, Mollet G, Schapiro D, Daugeron M-C, Tan W, et al.: Mutations in KEOPS-
592 complex genes cause nephrotic syndrome with primary microcephaly. *Nature genetics* 49:
593 1529–1538, 2017
594 14. Hayashi K, Hishikawa A, Hashiguchi A, Azegami T, Yoshimoto N, Nakamichi R, et al.:
595 Association of glomerular DNA damage and DNA methylation with one-year eGFR decline in IgA
596 nephropathy. *Sci Rep-uk* 10: 237, 2020

597 15. Hishikawa A, Hayashi K, Yoshimoto N, Nakamichi R, Homma K, Itoh H: DNA damage and
598 expression of DNA methylation modulators in urine-derived cells of patients with hypertension
599 and diabetes. *Sci Rep-uk* 10: 3377, 2020
600 16. Apelt K, White SM, Kim HS, Yeo J-E, Kragten A, Wondergem AP, et al.: ERCC1 mutations
601 impede DNA damage repair and cause liver and kidney dysfunction in patients. *J Exp Med* 218:
602 2020
603 17. Reiling JH, Hafen E: The hypoxia-induced paralogs Scylla and Charybdis inhibit growth by
604 down-regulating S6K activity upstream of TSC in Drosophila. *Gene Dev* 18: 2879–2892, 2004
605 18. Budanov AV, Karin M: p53 Target Genes Sestrin1 and Sestrin2 Connect Genotoxic Stress
606 and mTOR Signaling. *Cell* 134: 451–460, 2008
607 19. Wu D-D, Gao Y-R, Li T, Wang D-Y, Lu D, Liu S-Y, et al.: PEST-containing nuclear protein
608 mediates the proliferation, migration, and invasion of human neuroblastoma cells through MAPK
609 and PI3K/AKT/mTOR signaling pathways. *Bmc Cancer* 18: 499, 2018
610 20. Chebel A, Catallo R, Mabon C, Bachy E, Wenner T, Salles G, et al.: Rapamycin safeguards
611 lymphocytes from DNA damage accumulation in vivo. *European journal of cell biology* 95: 331–
612 341, 2016
613 21. Dominick G, Bowman J, Li X, Miller RA, Garcia GG: mTOR regulates the expression of DNA
614 damage response enzymes in long-lived Snell dwarf, GHRKO, and PAPPA-KO mice. *Aging Cell*
615 16: 52–60, 2016
616 22. Xie X, Hu H, Tong X, Li L, Liu X, Chen M, et al.: The mTOR–S6K pathway links growth
617 signalling to DNA damage response by targeting RNF168. *Nat Cell Biol* 20: 320–331, 2018
618 23. Zschiedrich S, Bork T, Liang W, Wanner N, Eulenbruch K, Munder S, et al.: Targeting mTOR
619 Signaling Can Prevent the Progression of FSGS. *Journal of the American Society of*
620 *Nephrology : JASN* 28: 2144–2157, 2017
621 24. Nishizono R, Kikuchi M, Wang SQ, Chowdhury M, Nair V, Hartman J, et al.: FSGS as an
622 Adaptive Response to Growth-Induced Podocyte Stress. *Journal of the American Society of*
623 *Nephrology : JASN* 28: 2931–2945, 2017
624 25. Puelles VG, Wolde JW van der, Wanner N, Scheppach MW, Cullen-McEwen LA, Bork T, et
625 al.: mTOR-mediated podocyte hypertrophy regulates glomerular integrity in mice and humans.
626 *Jci Insight* 4: e99271, 2019
627 26. Inoki K, Mori H, Wang J, Suzuki T, Hong S, Yoshida S, et al.: mTORC1 activation in
628 podocytes is a critical step in the development of diabetic nephropathy in mice. *The Journal of*
629 *clinical investigation* 121: 2181–2196, 2011
630 27. Kurayama R, Ito N, Nishibori Y, Fukuhara D, Akimoto Y, Higashihara E, et al.: Role of amino
631 acid transporter LAT2 in the activation of mTORC1 pathway and the pathogenesis of crescentic
632 glomerulonephritis. *Lab Invest* 91: 992–1006, 2011
633 28. Dittrich E, Schmaldienst S, Soleiman A, Horl WH, Pohanka E: Rapamycin-associated post-
634 transplantation glomerulonephritis and its remission after reintroduction of calcineurin-inhibitor
635 therapy. *Transplant Int* 17: 215–220, 2004
636 29. Butani L: Investigation of Pediatric Renal Transplant Recipients with Heavy Proteinuria after
637 Sirolimus Rescue. *Transplantation* 78: 1362–1366, 2004
638 30. Izzedine H, Brocheriou I, Frances C: Post-Transplantation Proteinuria and Sirolimus. *New*
639 *Engl J Med* 353: 2088–2089, 2005
640 31. Sennesael JJ, Bosmans JL, Bogers JP, Verbeelen D, Verpooten GA: Conversion from
641 Cyclosporine to Sirolimus in Stable Renal Transplant Recipients. *Transplantation* 80: 1578–
642 1585, 2005
643 32. Letavernier E, Bruneval P, Mandet C, Huyen J-PDV, Péraldi M-N, Helal I, et al.: High
644 Sirolimus Levels May Induce Focal Segmental Glomerulosclerosis De Novo. *Clin J Am Soc*
645 *Nephro* 2: 326–333, 2007

646 33. Cho ME, Hurley JK, Kopp JB: Sirolimus Therapy of Focal Segmental Glomerulosclerosis Is
647 Associated With Nephrotoxicity. *Am J Kidney Dis* 49: 310–317, 2007
648 34. Hochegger K, Jansky GL, Soleiman A, Wolf AM, Tagwerker A, Seger C, et al.: Differential
649 Effects of Rapamycin in Anti-GBM Glomerulonephritis. *J Am Soc Nephrol* 19: 1520–1529, 2008
650 35. Liberzon A, Birger C, Thorvaldsdóttir H, Ghandi M, Mesirov JP, Tamayo P: The Molecular
651 Signatures Database Hallmark Gene Set Collection. *Cell Syst* 1: 417–425, 2015
652 36. Cohen CD, Frach K, Schlöndorff D, Kretzler M: Quantitative gene expression analysis in
653 renal biopsies: A novel protocol for a high-throughput multicenter application. *Kidney Int* 61:
654 133–140, 2002
655 37. Cohen CD, Klingenhoff A, Boucherot A, Nitsche A, Henger A, Brunner B, et al.: Comparative
656 promoter analysis allows de novo identification of specialized cell junction-associated proteins.
657 *Proc National Acad Sci* 103: 5682–5687, 2006
658 38. Tusher VG, Tibshirani R, Chu G: Significance analysis of microarrays applied to the ionizing
659 radiation response. *Proceedings of the National Academy of Sciences of the United States of*
660 *America* 98: 5116–5121, 2001
661 39. Rinschen MM, Gödel M, Grahammer F, Zschiedrich S, Helmstädter M, Kretz O, et al.: A
662 Multi-layered Quantitative In Vivo Expression Atlas of the Podocyte Unravels Kidney Disease
663 Candidate Genes. *Cell reports* 23: 2495–2508, 2018
664 40. Mariani LH, Eddy S, AlAkwaa FM, McCown PJ, Harder JL, Martini S, et al.: Multidimensional
665 Data Integration Identifies Tumor Necrosis Factor Activation in Nephrotic Syndrome: A Model for
666 Precision Nephrology. *Medrxiv* 2021.09.09.21262925, 2021
667 41. Puelles VG, Douglas-Denton RN, Cullen-McEwen LA, Li J, Hughson MD, Hoy WE, et al.:
668 Podocyte Number in Children and Adults: Associations with Glomerular Size and Numbers of
669 Other Glomerular Resident Cells. *J Am Soc Nephrol* 26: 2277–2288, 2015
670 42. Endlich N, Kliewe F, Kindt F, Schmidt K, Kotb AM, Artelt N, et al.: The transcription factor
671 Dach1 is essential for podocyte function. *J Cell Mol Med* 22: 2656–2669, 2018
672 43. Liebau MC, Braun F, Höpker K, Weitbrecht C, Bartels V, Müller R-U, et al.: Dysregulated
673 Autophagy Contributes to Podocyte Damage in Fabry's Disease. *Plos One* 8: e63506, 2013
674 44. Shankland SJ, Pippin JW, Reiser J, Mundel P: Podocytes in culture: past, present, and
675 future. *Kidney international* 72: 26–36, 2007
676 45. Shabalin AA: Matrix eQTL: ultra fast eQTL analysis via large matrix operations.
677 *Bioinformatics* 28: 1353–1358, 2012
678 46. Stegle O, Parts L, Durbin R, Winn J: A Bayesian Framework to Account for Complex Non-
679 Genetic Factors in Gene Expression Levels Greatly Increases Power in eQTL Studies. *Plos*
680 *Comput Biol* 6: e1000770, 2010
681 47. Wen X, Lee Y, Luca F, Pique-Regi R: Efficient Integrative Multi-SNP Association Analysis via
682 Deterministic Approximation of Posteriors. *Am J Hum Genetics* 98: 1114–1129, 2016
683 48. Niedernhofer LJ, Garinis GA, Raams A, Lalai AS, Robinson AR, Appeldoorn E, et al.: A new
684 progeroid syndrome reveals that genotoxic stress suppresses the somatotroph axis. *Nature* 444:
685 1038–1043, 2006
686 49. Doig J, Anderson C, Lawrence NJ, Selfridge J, Brownstein DG, Melton DW: Mice with skin-
687 specific DNA repair gene (Ercc1) inactivation are hypersensitive to ultraviolet irradiation-induced
688 skin cancer and show more rapid actinic progression. *Oncogene* 25: 6229–6238, 2006
689 50. Karakasilioti I, Kamileri I, Chatzinikolaou G, Kosteas T, Vergadi E, Robinson AR, et al.: DNA
690 Damage Triggers a Chronic Autoinflammatory Response, Leading to Fat Depletion in NER
691 Progeria. *Cell Metabolism* 18: 403–415, 2013
692 51. Weeda G, Donker I, Wit J de, Morreau H, Janssens R, Vissers CJ, et al.: Disruption of
693 mouse ERCC1 results in a novel repair syndrome with growth failure, nuclear abnormalities and
694 senescence. *Current biology : CB* 7: 427–439, 1997

695 52. Moeller MJ, Sanden SK, Soofi A, Wiggins RC, Holzman LB: Podocyte-specific expression of
696 cre recombinase in transgenic mice. *Genesis (New York, N.Y. : 2000)* 35: 39–42, 2003
697 53. Birkisdóttir MB, Jaarsma D, Brandt RMC, Barnhoorn S, Vliet N, Imholz S, et al.: Unlike
698 dietary restriction, rapamycin fails to extend lifespan and reduce transcription stress in progeroid
699 DNA repair-deficient mice. *Aging Cell* 20: e13302, 2021
700 54. Bork T, Liang W, Yamahara K, Lee P, Tian Z, Liu S, et al.: Podocytes maintain high basal
701 levels of autophagy independent of mtor signaling. *Autophagy* 16: 1–17, 2019
702 55. Settembre C, Fraldi A, Medina DL, Ballabio A: Signals from the lysosome: a control centre
703 for cellular clearance and energy metabolism. *Nature Reviews Molecular Cell Biology* 14: 283–
704 296, 2013
705 56. Hirooka M, Hirota M, Kamada M: Renal lesions in Cockayne syndrome. *Pediatr Nephrol* 2:
706 239–243, 1988
707 57. Chehida AB, Ghali N, Abdelaziz RB, Moussa FB, Tebib N: Renal Involvement in 2 Siblings
708 With Cockayne Syndrome. *Iran J Kidney Dis* 11: 253–255, 2017
709 58. Faridounnia M, Wienk H, Kovačič L, Folkers GE, Jaspers NGJ, Kaptein R, et al.: The
710 Cerebro-Oculo-Facio-Skeletal (COFS) Syndrome point mutation F231L in the ERCC1 DNA
711 repair protein causes dissociation of the ERCC1-XPF complex. *Journal of Biological Chemistry*
712 2015
713 59. Kondo D, Noguchi A, Tamura H, Tsuchida S, Takahashi I, Kubota H, et al.: Elevated Urinary
714 Levels of 8-Hydroxy-2'-deoxyguanosine in a Japanese Child of Xeroderma
715 Pigmentosum/Cockayne Syndrome Complex with Infantile Onset of Nephrotic Syndrome.
716 *Tohoku J Exp Medicine* 239: 231–5, 2016
717 60. Hecker A, Graille M, Madec E, Gadelle D, Le Cam E, van Tilbergh H, et al.: The universal
718 Kae1 protein and the associated Bud32 kinase (PRPK), a mysterious protein couple probably
719 essential for genome maintenance in Archaea and Eukarya. *Biochem Soc T* 37: 29–35, 2009
720 61. Hishikawa A, Hayashi K, Abe T, Kaneko M, Yokoi H, Azegami T, et al.: Decreased KAT5
721 Expression Impairs DNA Repair and Induces Altered DNA Methylation in Kidney Podocytes. *Cell*
722 *reports* 26: 1318-1332.e4, 2019
723 62. Schermer B, Bartels V, Frommolt P, Habermann B, Braun F, Schultze JL, et al.:
724 Transcriptional profiling reveals progeroid Ercc1-/Δ mice as a model system for glomerular
725 aging. *Bmc Genomics* 14: 559, 2013
726 63. Gödel M, Hartleben B, Herbach N, Liu S, Zschiedrich S, Lu S, et al.: Role of mTOR in
727 podocyte function and diabetic nephropathy in humans and mice. *The Journal of clinical*
728 *investigation* 121: 2197–2209, 2011
729 64. Ising C, Koehler S, Brähler S, Merkwirth C, Höhne M, Baris OR, et al.: Inhibition of
730 insulin/IGF-1 receptor signaling protects from mitochondria-mediated kidney failure. *EMBO*
731 *Molecular Medicine* 7: 275–287, 2015
732 65. Mulderrig L, Garaycoechea JI: XPF-ERCC1 protects liver, kidney and blood homeostasis
733 outside the canonical excision repair pathways. *Plos Genet* 16: e1008555, 2020
734 66. Milanese C, Bombardieri CR, Sepe S, Barnhoorn S, Payán-Goméz C, Caruso D, et al.: DNA
735 damage and transcription stress cause ATP-mediated redesign of metabolism and potentiation
736 of anti-oxidant buffering. *Nat Commun* 10: 4887, 2019

737

738 **Acknowledgments:**

739 The excellent technical expertise of Martyna Brütting, Melanie Schaper, Anja Obser, Ilka
740 Edenhofer and Bhawani Nagarajah is gratefully acknowledged. The DNA damage response
741 inhibitors used in this study were a kind gift of Ron Jachimowicz. All schematics in figures were

742 created with BioRender.com. The ERCB-KFB was supported by the Else Kröner-Fresenius
743 Foundation. We also thank all participating centres of the European Renal cDNA Bank - Kröner-
744 Fresenius biopsy bank (ERCB-KFB) and their patients for their cooperation. Active members at
745 the time of the study see (N. Shved et al., Scientific reports 7, 8576 (2017)). The Nephrotic
746 Syndrome Rare Disease Clinical Research Network III (NEPTUNE) is part of the Rare Diseases
747 Clinical Research Network (RDCRN), which is funded by the National Institutes of Health (NIH)
748 and led by the National Center for Advancing Translational Sciences (NCATS) through its Office
749 of Rare Diseases Research (ORDR). NEPTUNE is funded under grant number U54DK083912 as
750 a collaboration between NCATS and the National Institute of Diabetes and Digestive and Kidney
751 Diseases (NIDDK). Additional funding and/or programmatic support for this project has also been
752 provided by the University of Michigan, NephCure Kidney International and the Halpin Foundation.
753 All RDCRN consortia are supported by the network's Data Management and Coordinating Center
754 (DMCC) (U2CTR002818). Funding support for the DMCC is provided by NCATS and the National
755 Institute of Neurological Disorders and Stroke (NINDS).
756 Members of the Nephrotic Syndrome Study Network (NEPTUNE)
757 **Members of the Nephrotic Syndrome Study Network (NEPTUNE)**
758 NEPTUNE Enrolling Centers
759 *Cleveland Clinic, Cleveland, OH*: K Dell[*], J Sedor[**], M Schachere[#], J Negrey[#]
760 *Children's Hospital, Los Angeles, CA*: K Lemley[*], S Tang[#]
761 *Children's Mercy Hospital, Kansas City, MO*: T Srivastava[*], S Morrison[#]
762 *Cohen Children's Hospital, New Hyde Park, NY:* C Sethna[*], M Pfaiff [#]
763 *Columbia University, New York, NY:* P Canetta[*], A Pradhan[#]
764 *Emory University, Atlanta, GA:* L Greenbaum[*], C Wang**, E Yun[#]
765 *Harbor-University of California Los Angeles Medical Center:* S Adler[*], J LaPage[#]
766 *John H. Stroger Jr. Hospital of Cook County, Chicago, IL:* A Athavale[*], M Itteera
767 *Johns Hopkins Medicine, Baltimore, MD:* M Atkinson[*], T Dell[#]
768 *Mayo Clinic, Rochester, MN:* F Fervenza[*], M Hogan**, J Lieske[*], V Chernitskiy[#]
769 *Montefiore Medical Center, Bronx, NY:* F Kaskel[*], M Ross[*], P Flynn[#]
770 *NIDDK Intramural, Bethesda MD:* J Kopp[*], J Blake[#]
771 *New York University Medical Center, New York, NY:* L Malaga-Dieguez[*], O Zhdanova**, F
772 Modersitzki[#], L Pehrson[#]
773 *Stanford University, Stanford, CA:* R Lafayette[*], B Yeung[#]
774 *Temple University, Philadelphia, PA:* I Lee[*], S Quinn-Boyle[#]

775 *University Health Network Toronto:* H Reich *, M Hladunewich**, P Ling[#], M Romano[#]
776 *University of Miami, Miami, FL:* A Fornoni[*], C Bidot[#]
777 *University of Michigan, Ann Arbor, MI:* M Kretzler[*], D Gipson*, A Williams[#], C Klida[#]
778 *University of North Carolina, Chapel Hill, NC:* V Derebail[*], K Gibson[*], A Froment[#], S Kelley[#]
779 *University of Pennsylvania, Philadelphia, PA:* L Holzman[*], K Meyers**, K Kallem[#], A Swenson[#]
780 *University of Texas Southwestern, Dallas, TX:* K Sambandam[*], K Aleman[#], M Rogers[#]
781 *University of Washington, Seattle, WA:* A Jefferson[*], S Hingorani**, K Tuttle**[§], M Bray [#], E Pao[#],
782 A Cooper[#§]
783 *Wake Forest University Baptist Health, Winston-Salem, NC:* JJ Lin*, Stefanie Baker[#]
784
785 *Data Analysis and Coordinating Center*: M Kretzler*, L Barisoni**, C Gadegbeku**, B Gillespie**,
786 D Gipson**, L Holzman**, L Mariani**, M Sampson**, J Sedor**, J Zee**, G Alter, H Desmond, S
787 Eddy, D Fermin, M Larkina, S Li, S Li, CC Lienczewski, T Mainieri, R Scherr, A Smith, A
788 Szymanski, A Williams.
789
790 *Digital Pathology Committee*: Carmen Avila-Casado (University Health Network, Toronto), Serena
791 Bagnasco (Johns Hopkins University), Joseph Gaut (Washington University in St Louis), Stephen
792 Hewitt (National Cancer Institute), Jeff Hodgin (University of Michigan), Kevin Lemley (Children's
793 Hospital of Los Angeles), Laura Mariani (University of Michigan), Matthew Palmer (University of
794 Pennsylvania), Avi Rosenberg (Johns Hopkins University), Virginie Royal (University of Montreal),
795 David Thomas (University of Miami), Jarcy Zee (University of Pennsylvania) Co-Chairs: Laura
796 Barisoni (Duke University) and Cynthia Nast (Cedar Sinai).
797
798 *Principal Investigator; **Co-investigator; [#]Study Coordinator
799 [§]Providence Medical Research Center, Spokane, WA
800
801 **Figures and Figure Legends:**

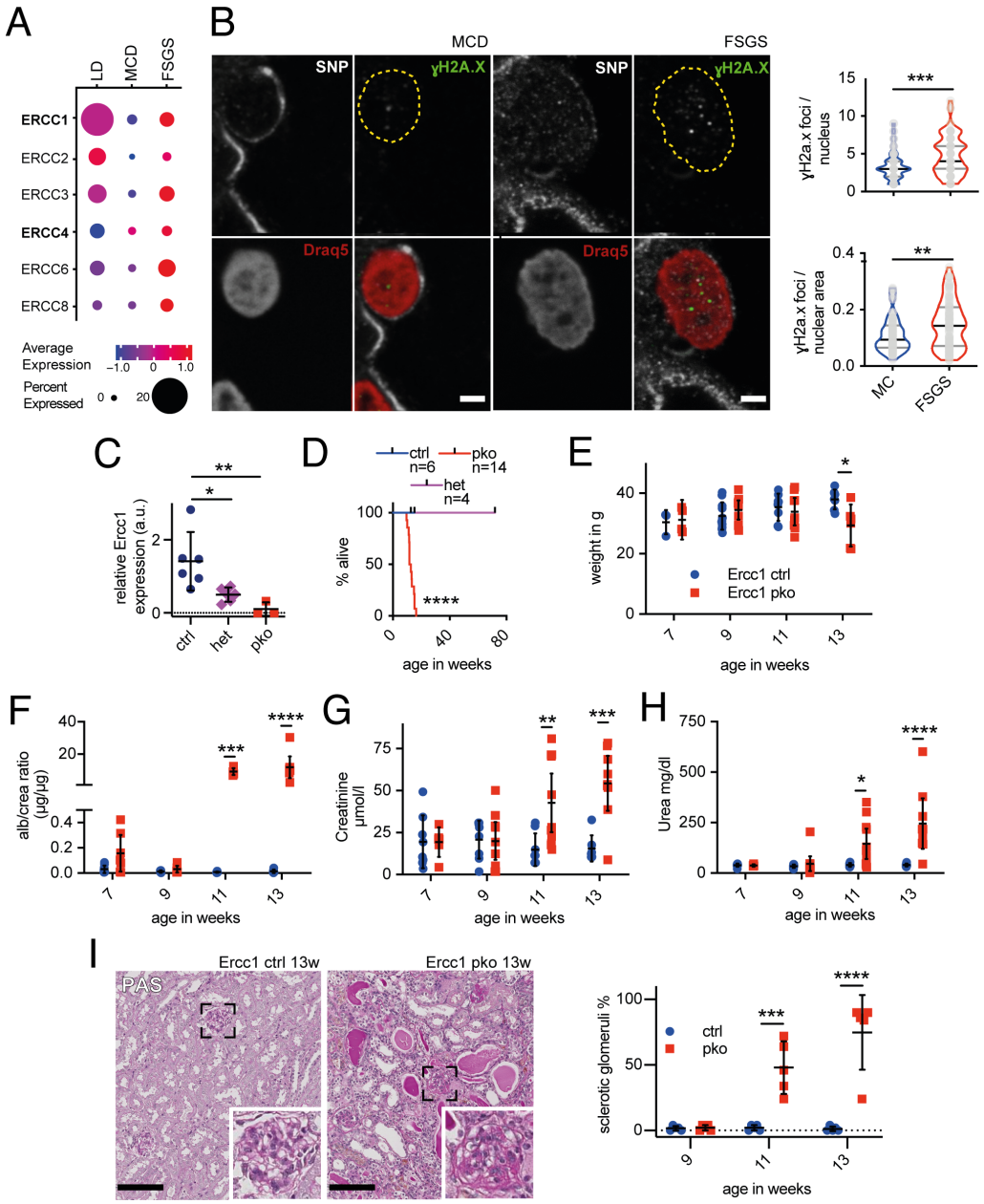
A
LD
MCD
FSGS
ERCC1
ERCC2
ERCC3
ERCC4
ERCC6
ERCC8
Average Expression
−1.0
0
1.0
Percent Expressed
0
20
B
MCD
FSGS
SNP
γH2A.X
Draq5
γH2a.x foci / nucleus
γH2a.x foci / nuclear area
MC
FSGS
C
relative Ercc1 expression (a.u.)
ctrl
het
pko
D
ctrl n=6
pko n=14
het n=4
% alive
age in weeks
E
weight in g
Ercc1 ctrl
Ercc1 pko
age in weeks
F
alb/crea ratio (µg/µg)
age in weeks
G
Creatinine µmol/l
age in weeks
H
Urea mg/dl
age in weeks
I
Ercc1 ctrl 13w
Ercc1 pko 13w
PAS
sclerotic glomeruli %
ctrl
pko
age in weeks

802

803 **Figure 1: Nucleotide excision repair (NER) gene expression is perturbed in human FSGS and this**
804 **perturbation causes glomerulosclerosis**
805 A: Bubble plot indicating the differences in Ercc gene expression in podocytes between living donor (LD)
806 kidney samples, Minimal change disease (MCD) and FSGS biopsies obtained through single nucleus
807 sequencing.
808 B: Representative immunofluorescence staining of synaptopodin (SNP), γH2A.X and Draq5 in sections of
809 human MCD and FSGS biopsies with quantification of γH2A.X foci per podocyte nucleus, scalebar
810 indicating 2 μm, yellow dotted line indicating nuclear border, n=4, 4 glomeruli per sample, 5 podocytes per
811 glomerulus.
812 C: qPCR analysis for *Ercc1* in FACS-sorted podocytes of *Ercc1* ctrl, wt/pko (het) or pko mice. Delta-Delta-
813 CT values expressed as scatterplots depicting mean plus 95% confidence interval.
814 D: Kaplan-Meyer curve depicting survival of *Ercc1* ctrl, wt/pko (het) and pko mice (Mantel-Cox test).
815 E: Weight analysis; F: urinary albumin/creatinine analysis; G: serum creatinine analysis; H: serum urea
816 analysis of *Ercc1* ctrl and pko mice.
817 I: Representative Periodic Acid Schiff (PAS) staining of 13-week-old *Ercc1* ctrl and pko mice and
818 quantification of sclerotic glomeruli, scalebars: 100 μm, n = 5, 50 glomeruli per sample.
819 All violin plots indicate median (black) and upper and lower quartile (gray), scatterplots indicate mean plus
820 95% confidence interval, *$p \leq 0{,}05$, **$p \leq 0{,}01$, ***$p \leq 0{,}001$, ****$p \leq 0{,}0001$.
821

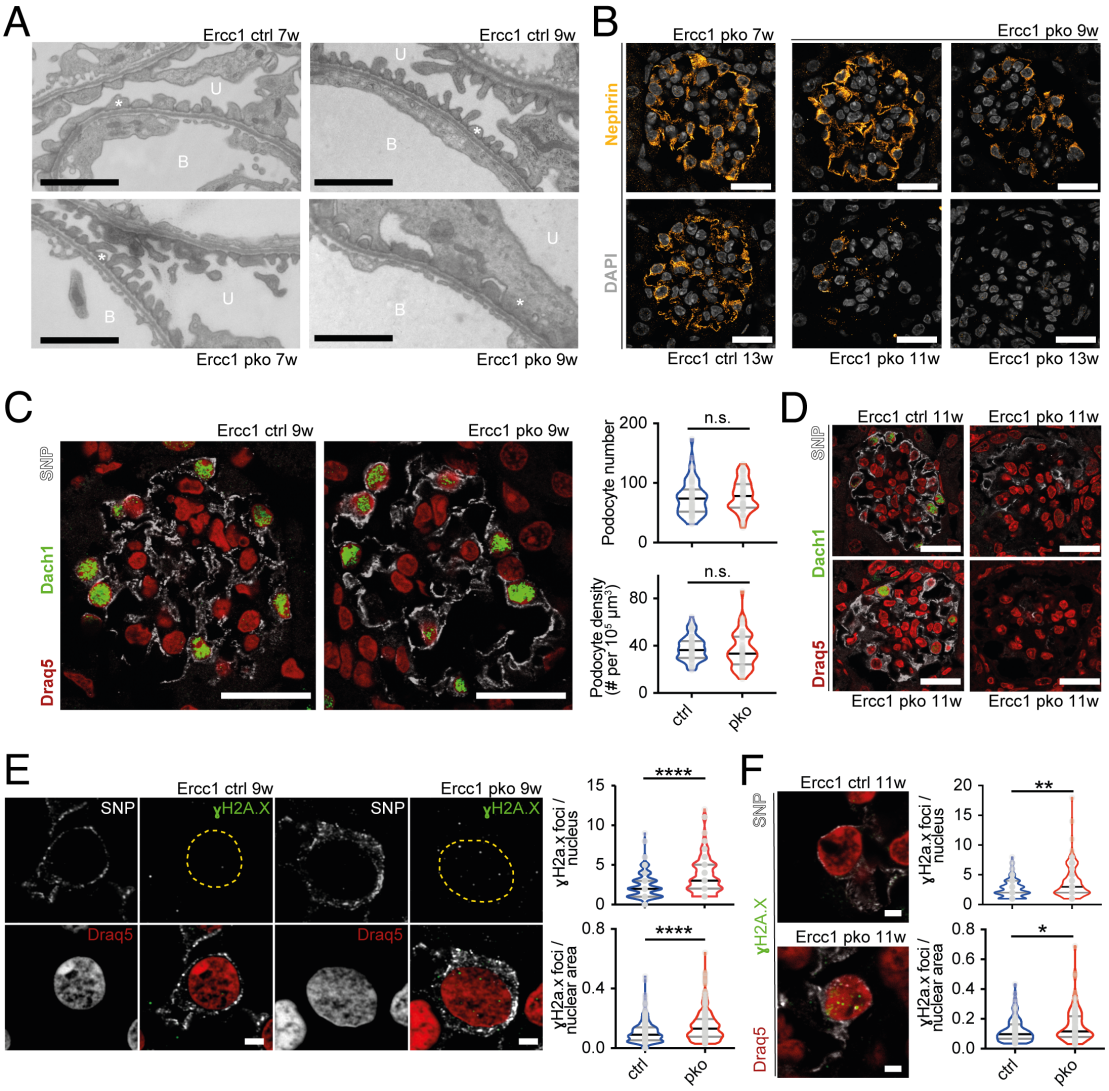
A
Ercc1 ctrl 7w
Ercc1 ctrl 9w
Ercc1 pko 7w
Ercc1 pko 9w
U
B
*
B
Nephrin
DAPI
Ercc1 pko 7w
Ercc1 pko 9w
Ercc1 ctrl 13w
Ercc1 pko 11w
Ercc1 pko 13w
C
Ercc1 ctrl 9w
Ercc1 pko 9w
SNP
Dach1
Draq5
Podocyte number
n.s.
Podocyte density (# per 10^5 µm^3)
ctrl
pko
D
Ercc1 ctrl 11w
Ercc1 pko 11w
E
SNP
γH2A.X
Draq5
γH2a.x foci / nucleus
γH2a.x foci / nuclear area
****
F
**
*

822

823 **Figure 2: The podocyte-specific constitutive ko of *Ercc1* leads to foot process effacement and**
824 **podocyte loss accompanied by accumulation of DNA damage.**
825 A: Representative electron microscopy image of 7- and 9-week-old *Ercc1* ctrl and pko slit diaphragms,
826 scalebar indicating 2 μm, B: blood side – intracapillary space, U: urinary side – Bowman's space, asterisk
827 indicating podocyte foot process (n=3).
828 B: Representative immunofluorescence staining of slit diaphragm protein nephrin (yellow) with nuclear
829 marker DAPI (grey) of *Ercc1* ctrl at 13 weeks of age and pko kidneys at 7, 9, 11, and 13 weeks of age,
830 scalebar indicating 2 μm (n=5).
831 C: Representative immunofluorescence staining of podocyte proteins synaptopodin (SNP, gray),
832 Dachshund homolog 1 (Dach1, green) [42] and far-red fluorescent DNA dye Draq5 (red) as a nuclear marker
833 in sections of 9-week-old *Ercc1* ctrl and pko kidneys, with quantification of podocyte number and density of
834 *Ercc1* ctrl and pko kidneys, scalebar indicating 10 μm (n=5).
835 D: Corresponding staining of podocyte proteins synaptopodin (gray), Dachshund homolog 1 (Dach1, green)
836 [42] and far-red fluorescent DNA dye Draq5 (red) as a nuclear marker in paraffin-embedded sections of 11-
837 week-old *Ercc1* ctrl and pko kidneys, scalebar indicating 10 μm (n=5).
838 E: Representative immunofluorescence staining of synaptopodin (SNP, gray), DNA damage marker γH2A.X
839 (green) and nuclear marker Draq5 (red) in sections of 9-week-old *Ercc1* ctrl and pko kidneys, with
840 quantification of γH2A.X foci per podocyte nucleus and nuclear area of *Ercc1* ctrl and pko kidneys, scalebar
841 indicating 2 μm, yellow dotted line indicating nuclear border, n=5, 10 glomeruli per sample, 5 podocytes per
842 glomerulus.
843 F: Representative immunofluorescence staining of synaptopodin (SNP, gray), DNA damage marker γH2A.X
844 (green) and nuclear marker Draq5 (red) in sections of 11-week-old *Ercc1* ctrl and pko kidneys, with
845 quantification of γH2A.X foci per podocyte nucleus and nuclear area of *Ercc1* ctrl and pko kidneys, scalebar
846 indicating 2 μm, n=5, 10 glomeruli per sample, 5 podocytes per glomerulus.
847 All violin plots indicate median (black) and upper and lower quartile (gray), *$p \leq 0{,}05$, **$p \leq 0{,}01$, ***$p \leq$
848 $0{,}001$, ****$p \leq 0{,}0001$.
849

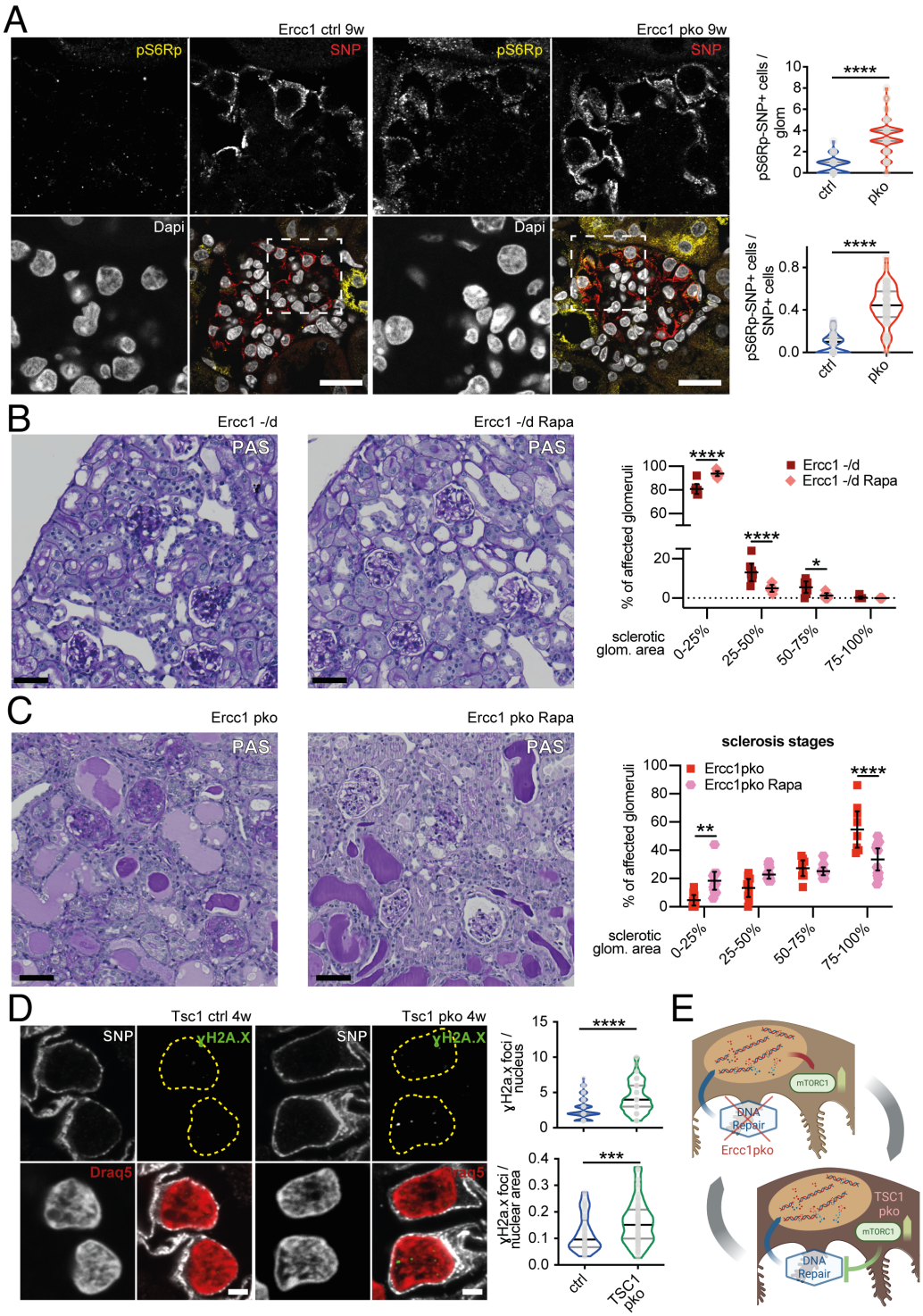
A
Ercc1 ctrl 9w
Ercc1 pko 9w
pS6Rp
SNP
Dapi
pS6Rp-SNP+ cells / glom
pS6Rp-SNP+ cells / SNP+ cells
****
ctrl
pko
B
Ercc1 -/d
Ercc1 -/d Rapa
PAS
% of affected glomeruli
sclerotic glom. area
0-25%
25-50%
50-75%
75-100%
*
C
Ercc1 pko
Ercc1 pko Rapa
sclerosis stages
Ercc1pko
Ercc1pko Rapa
**
D
Tsc1 ctrl 4w
Tsc1 pko 4w
γH2A.X
Draq5
γH2a.x foci / nucleus
γH2a.x foci / nuclear area
***
TSC1 pko
E
mTORC1
DNA Repair
Ercc1pko

850

851 **Figure 3: DNA damage leads to an activation of the mTORC1 pathway in podocytes *in vivo*.**
852 A: Representative immunofluorescence staining of SNP, pS6RP and DAPI in sections of 9-week-old *Ercc1*
853 ctrl and pko kidneys with quantification of SNP and pS6RP double positive cells per glomerulus and per
854 total SNP positive cells, scalebar indicating 10 μm (n=5, 10 glomeruli per sample).
855 B: Representative Periodic Acid Schiff (PAS) staining of end-of-life *Ercc1* -/delta mice treated with 14 mg
856 rapamycin per kg food from 8 weeks of age and quantification of sclerotic glomeruli (n = 8, 50 glomeruli per
857 sample), scalebar indicating 50 μm.
858 C: Representative Periodic Acid Schiff (PAS) staining of *Ercc1* pko mice treated with vehicle (*Ercc1* pko) or
859 rapamycin (*Ercc1* pko Rapa) from 6 weeks of age and quantification of sclerotic glomeruli, n ≥ 9, 50 glomeruli
860 per sample, scalebar indicating 50 μm.
861 D: Representative immunofluorescence staining of synaptopodin (SNP, gray), DNA damage marker γH2A.X
862 (green) and nuclear marker Draq5 (red) in sections of 4-week-old *Tsc1* ctrl and pko kidneys, with
863 quantification of γH2A.X foci per podocyte nucleus and nuclear area of *Ercc1* ctrl and pko kidneys, yellow
864 dotted line indicating nuclear border (n=5, 10 glomeruli per sample, 5 podocytes per glomerulus), scalebar
865 indicating 2 μm.
866 E: Schematic overview depicting the potential interplay between defective DNA damage repair and
867 increased mTORC1 signaling. In *Ercc1* pko mice, accumulation of DNA damage triggers mTORC1
868 signaling. In *Tsc1* pko mice, hyperactive mTORC1 signaling also leads to increased DNA damage foci.
869 All violin plots indicate median (black) and upper and lower quartile (gray), scatterplots indicate mean plus
870 95% confidence interval, *p ≤ 0,05, **p ≤ 0,01, ***p ≤ 0,001, ****p ≤ 0,0001.
871

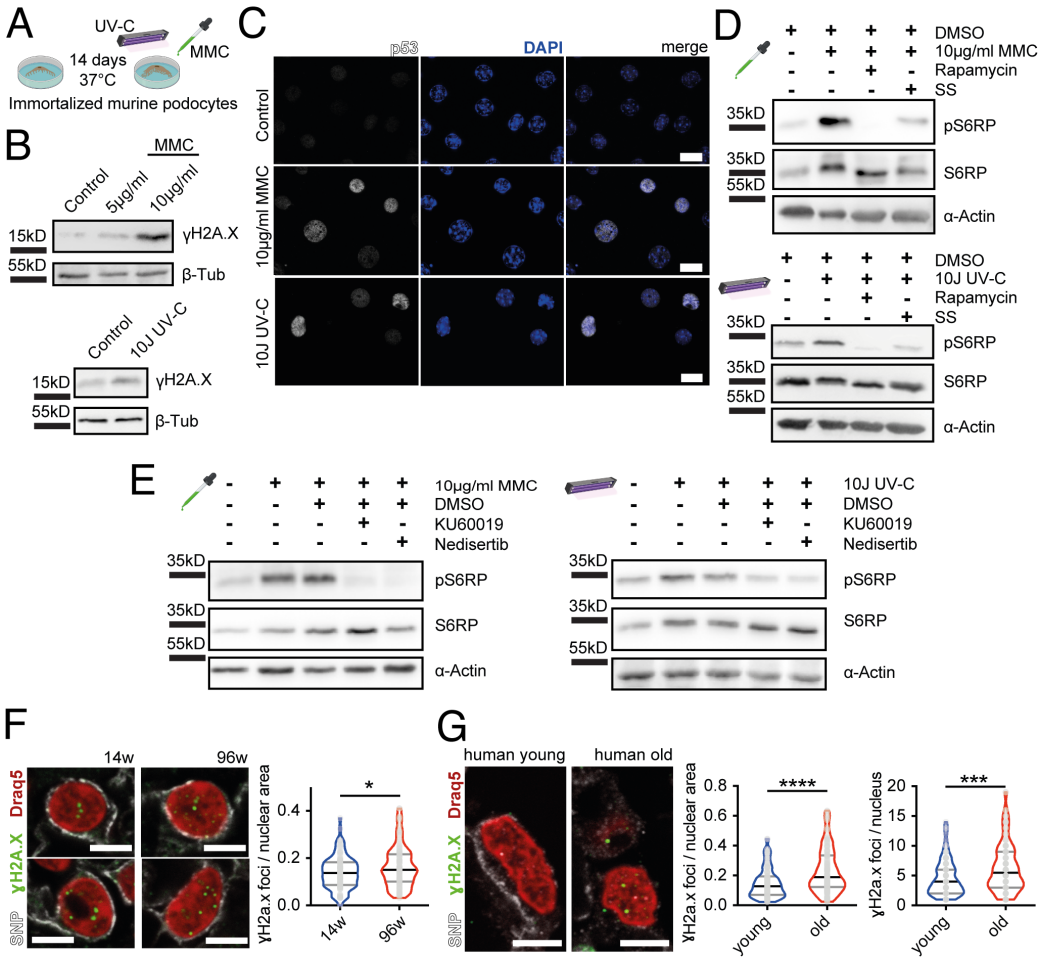
A
UV-C
MMC
14 days
37°C
Immortalized murine podocytes
B
MMC
Control
5µg/ml
10µg/ml
15kD
55kD
γH2A.X
β-Tub
Control
10J UV-C
15kD
55kD
γH2A.X
β-Tub
C
p53
DAPI
merge
Control
10µg/ml MMC
10J UV-C
D
DMSO
10µg/ml MMC
Rapamycin
SS
35kD
35kD
55kD
pS6RP
S6RP
α-Actin
DMSO
10J UV-C
Rapamycin
SS
35kD
35kD
55kD
pS6RP
S6RP
α-Actin
E
10µg/ml MMC
DMSO
KU60019
Nedisertib
35kD
35kD
55kD
pS6RP
S6RP
α-Actin
10J UV-C
DMSO
KU60019
Nedisertib
35kD
35kD
55kD
pS6RP
S6RP
α-Actin
F
14w
96w
Draq5
γH2A.X
SNP
γH2a.x foci / nuclear area
0.4
0.2
0.0
*
14w
96w
G
human young
human old
Draq5
γH2A.X
SNP
γH2a.x foci / nuclear area
0.8
0.6
0.4
0.2
0.0
****
young
old
γH2a.x foci / nucleus
20
15
10
5
0
***
young
old

872

873 **Figure 4: DNA damage leads to an activation of the mTORC1 pathway in podocytes *in vitro* through**
874 **a DNA-PK-dependent mechanism and podocytes accumulate DNA damage with aging.**
875 A: Schematic of *in vitro* protocol for the induction of DNA damage.
876 B: Representative immunoblot images for DNA damage marker γH2A.X and loading control protein beta-
877 tubulin of immortalized murine podocyte lysates (n=3).
878 C: Representative immunofluorescence images for tumor suppressor p53 and nuclear marker DAPI in
879 immortalized murine podocytes (n=3).
880 D: Representative immunoblot images for mTORC1 target phospho-S6 ribosomal protein (pS6RP), S6RP
881 and loading control protein alpha-actin of immortalized murine podocyte lysates (n=3).
882 All cells imaged or lysed after treatment with mitomycin C (MMC) or ultraviolet C (UV-C) irradiation ±
883 rapamycin or serum starvation (SS), n ≥ 4.
884 E: Representative immunoblot images for mTORC1 target phospho-S6 ribosomal protein (pS6RP), S6RP
885 and loading control protein alpha-actin of immortalized murine podocyte lysates (n=3 MMC; n=6 UV-C).
886 All cells imaged or lysed after treatment with mitomycin C (MMC) or ultraviolet C (UV-C) irradiation ± ATM
887 inhibitor KU60019 or DNA-PK inhibitor nedisertib.
888 F: Representative immunofluorescence staining of SNP, γH2A.X and Draq5 in sections of murine young
889 and aged wildtype kidneys with quantification of γH2A.X foci per podocyte nucleus, scalebar indicating 2
890 μm, n=4, 5 glomeruli per sample, 5 podocytes per glomerulus.
891 G: Representative immunofluorescence staining of SNP, γH2A.X and Draq5 in sections of human young
892 and old tumor nephrectomy kidneys with quantification of γH2A.X foci per podocyte nucleus, scalebar
893 indicating 5 μm, n≥4, 5 glomeruli per sample, 5 podocytes per glomerulus.
894 All violin plots indicate median (black) and upper and lower quartile (gray), *p ≤ 0,05, ***p ≤ 0,001, ****p ≤
895 0,0001.
896

897 **Supplementary Information:**

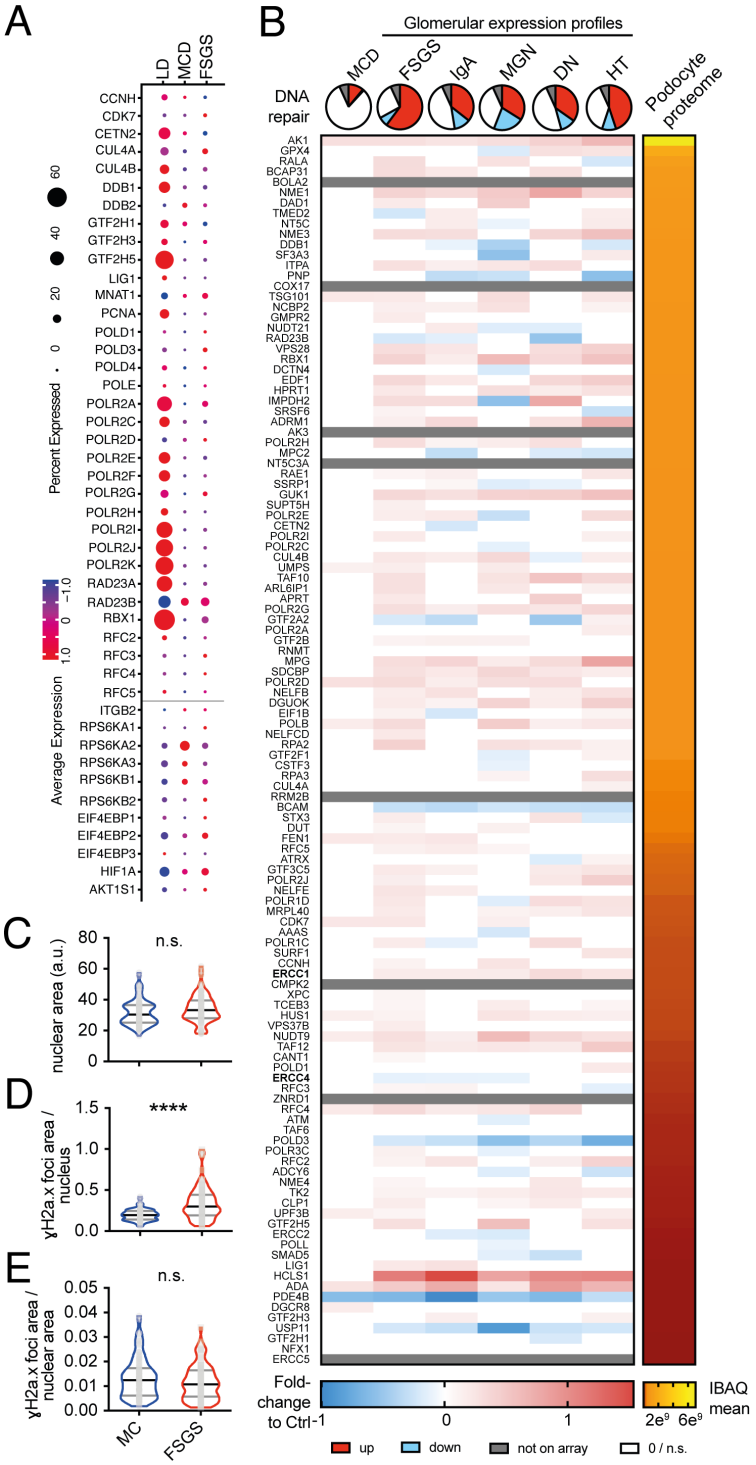
A
LD
MCD
FSGS
Percent Expressed
Average Expression
B
Glomerular expression profiles
MCD
FSGS
IgA
MGN
DN
HT
DNA repair
Podocyte proteome
Fold-change to Ctrl
IBAQ mean
up
down
not on array
0 / n.s.
C
nuclear area (a.u.)
n.s.
D
γH2a.x foci area / nucleus
****
E
γH2a.x foci area / nuclear area
n.s.
MC
FSGS

899 **Figure S1:**
900 A: Bubble plot indicating the differences in NER (excluding Ercc genes) and mTORC1 target gene
901 expression in podocytes between living donor (LD) kidney samples, Minimal change disease (MCD) and
902 FSGS biopsies obtained through single nucleus sequencing. Grey line indicating the split between NER and
903 mTORC1 target genes.
904 B: Expression profile of 118 hallmark DNA repair genes in MCD, FSGS, IgA nephropathy (IgA),
905 membranous nephropathy (MGN), diabetic nephropathy (DN), and hypertension (HT) glomeruli compared
906 to controls depicted as parts of whole and single genes in heatmaps. Genes ranked by their protein
907 abundance (Intensity-based absolute quantification - IBAQ) in murine podocyte proteome analysis[39].
908 C: Quantification of podocyte nuclear area of human MCD and FSGS biopsies (n=4, 4 glomeruli per sample,
909 5 podocytes per glomerulus).
910 D: Quantification of γH2A.X foci area per podocyte nucleus of human MCD and FSGS biopsies (n=4, 4
911 glomeruli per sample, 5 podocytes per glomerulus).
912 E: Quantification of γH2A.X foci area per podocyte nuclear area of human MCD and FSGS biopsies (n=4,
913 4 glomeruli per sample, 5 podocytes per glomerulus).
914 All violin plots indicate median (black) and upper and lower quartile (gray), ****$p \leq 0{,}0001$.

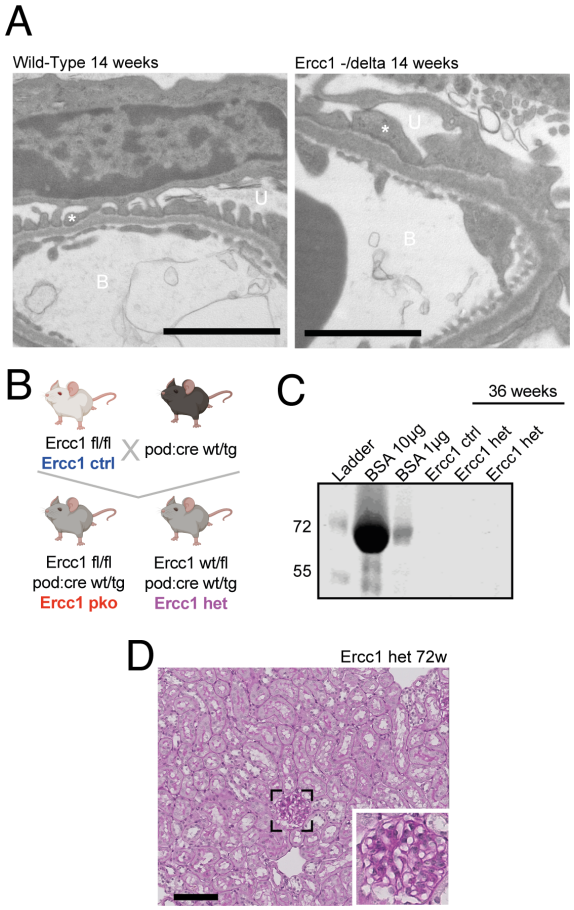
A
Wild-Type 14 weeks
Ercc1 -/delta 14 weeks
U
B
B
Ercc1 fl/fl
Ercc1 ctrl
pod:cre wt/tg
Ercc1 fl/fl
pod:cre wt/tg
Ercc1 pko
Ercc1 wt/fl
pod:cre wt/tg
Ercc1 het
C
36 weeks
Ladder
BSA 10µg
BSA 1µg
Ercc1 ctrl
Ercc1 het
Ercc1 het
72
55
D
Ercc1 het 72w

915

916 **Fig S2:**

917 A: Representative electron microscopy image of 14-week-old wild-type (WT) and *Ercc1* -/delta (Ercc1-/d)
918 glomerular filtration barrier, scalebar indicating 2 μm, B: blood side – intracapillary space, U: urinary side –
919 bowman's space, Asterisk indicating podocyte foot process (n=4).
920 B: Breeding scheme for homozygous and heterozygous podocyte-specific *Ercc1* pko mice.
921 C: Representative Coomassie blue staining of *Ercc1* ctrl and wt/pko (het) urine at 36 weeks of age; bovine
922 serum albumin (BSA) was loaded as reference.
923 D: Representative Periodic Acid Schiff (PAS) staining of *Ercc1* wt/pko (het) kidney at 72 weeks of age,
924 scalebar: 100 μm.

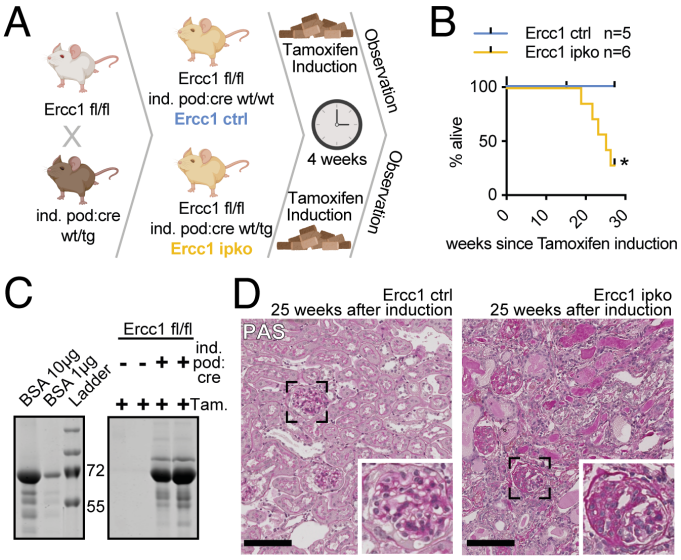
A
Ercc1 fl/fl
X
ind. pod:cre wt/tg
Ercc1 fl/fl
ind. pod:cre wt/wt
Ercc1 ctrl
Ercc1 fl/fl
ind. pod:cre wt/tg
Ercc1 ipko
Tamoxifen Induction
4 weeks
Tamoxifen Induction
Observation
Observation
B
Ercc1 ctrl n=5
Ercc1 ipko n=6
% alive
100
50
0
0
10
20
30
weeks since Tamoxifen induction
C
BSA 10µg
BSA 1µg
Ladder
Ercc1 fl/fl
ind. pod: cre
- - + +
+ + + +Tam.
72
55
D
Ercc1 ctrl
25 weeks after induction
Ercc1 ipko
25 weeks after induction
PAS

925

926 **Figure S3:**
927 A: Breeding and induction scheme for homozygous inducible podocyte-specific *Ercc1* ko mice (ipko).
928 B: Kaplan-Meyer curve depicting survival of *Ercc1* ctrl and ipko mice (Mantel-Cox test).
929 C: Representative Coomassie blue staining of *Ercc1* ctrl and ipko urine 18 weeks after induction with
930 tamoxifen; bovine serum albumin (BSA) was loaded as reference (n=6).
931 D: Representative Periodic Acid Schiff (PAS) staining of *Ercc1* ctrl and ipko mice 25 weeks after induction
932 with tamoxifen (n=6).
933 *$p \leq 0{,}05$, scalebars: 100μm.

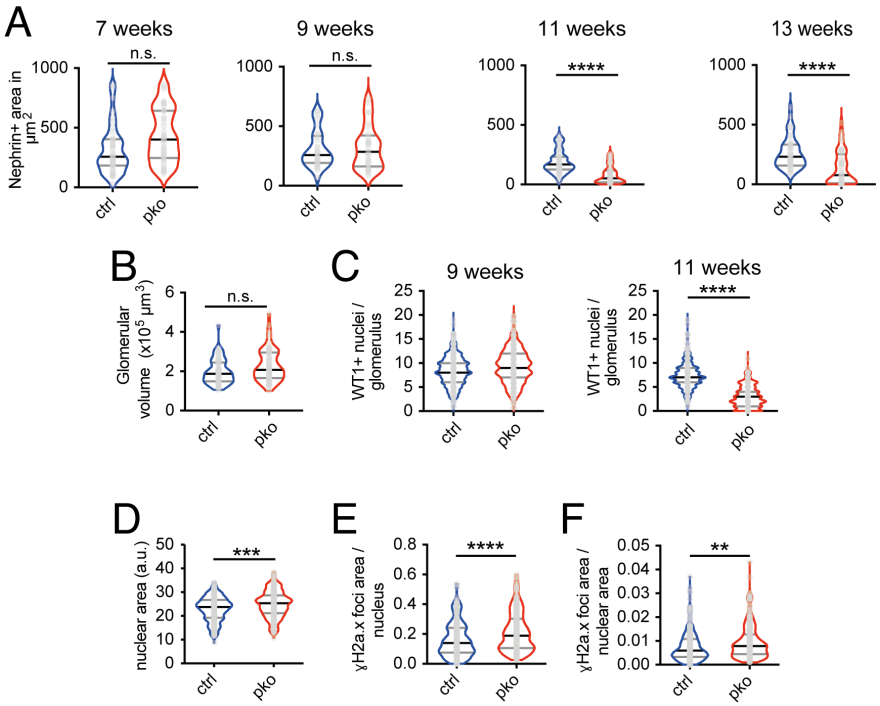
A
7 weeks
9 weeks
11 weeks
13 weeks
Nephrin+ area in µm²
n.s.
n.s.
****
****
ctrl
pko
B
Glomerular volume (x10⁵ µm³)
n.s.
C
9 weeks
11 weeks
WT1+ nuclei / glomerulus
****
D
nuclear area (a.u.)
***
E
γH2a.x foci area / nucleus
****
F
γH2a.x foci area / nuclear area
**

934

935 **Figure S4:**
936 A: Quantification of nephrin positive area in μm^2 of *Ercc1* ctrl and pko kidneys at 7, 9, 11, and 13 weeks of
937 age, n=4, 10 glomeruli per sample.
938 B: Quantification of glomerular volume of 9-week-old *Ercc1* ctrl and pko kidneys, n = 5, 10 glomeruli per
939 sample.
940 C: Quantification of WT+ nuclei per glomerulus of *Ercc1* ctrl and pko kidneys at 9 and 11 weeks of age, n =
941 4, ≥50 glomeruli per group
942 D: Quantification of podocyte nuclear are of 9-week-old *Ercc1* ctrl and pko kidneys, n = 5, 10 glomeruli per
943 sample, 5 podocytes per glomerulus.
944 E: Quantification of γH2A.X foci area per podocyte nucleus of 9-week-old *Ercc1* ctrl and pko kidneys, n = 5,
945 10 glomeruli per sample, 5 podocytes per glomerulus.
946 F: Quantification of γH2A.X foci area per podocyte nuclear area of 9-week-old *Ercc1* ctrl and pko kidneys,
947 n = 5, 10 glomeruli per sample, 5 podocytes per glomerulus.
948 All violin plots indicate median (black) and upper and lower quartile (gray), **p ≤ 0,01, ***p ≤ 0,001, ****p ≤
949 0,0001.

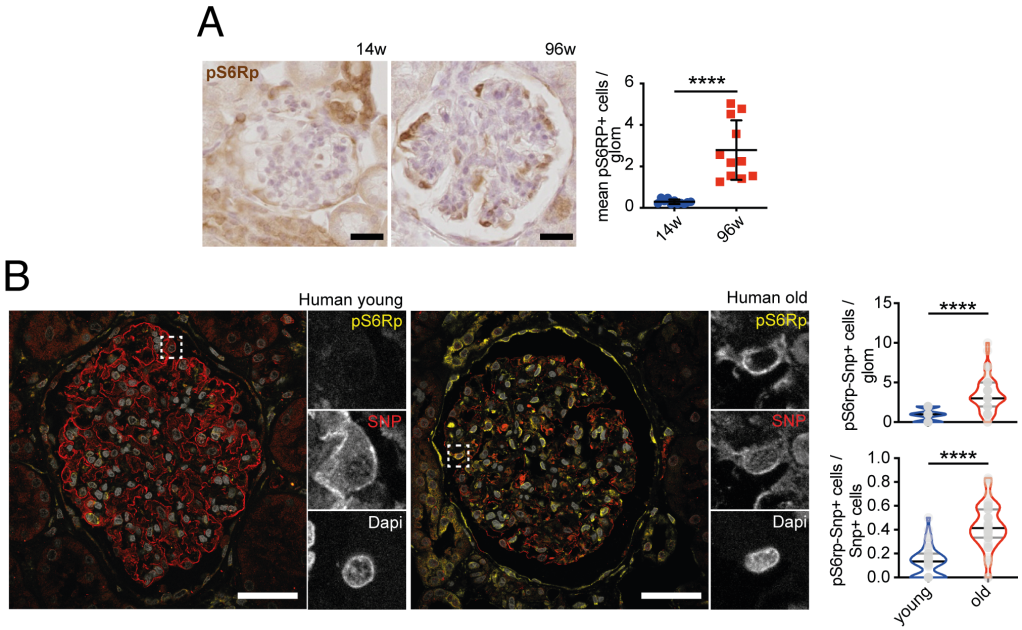
A
14w
96w
pS6Rp
mean pS6RP+ cells / glom
****
14w
96w
B
Human young
Human old
pS6Rp
SNP
Dapi
pS6rp-Snp+ cells / glom
pS6rp-Snp+ cells / Snp+ cells
young
old

950

951 **Figure S5:**
952 A: Representative immunohistochemistry staining of pS6RP in sections of murine young and aged wildtype
953 kidneys with quantification of pS6RP-positive cells per glomerulus, scalebar indicating 25 μm, n =11, 50
954 glomeruli per sample.
955 B: Representative immunofluorescence staining of SNP, pS6RP and DAPI in sections of young and old
956 human tumor nephrectomy kidneys with quantification of SNP and pS6RP double positive cells per
957 glomerulus and per total SNP positive cells, scalebar indicating 10 μm, n=≥4, 10 glomeruli per sample.
958 Scatterplot depicting mean and 95% confidence interval, all violin plots indicating median (black) and upper
959 and lower quartile (gray), ****p ≤ 0,0001.
960

961 **Table S1: Gene expression analysis of ERCB for Hallmark DNA Repair and Nucleotide Excision**
962 **Repair Genes**
963

964 **Table S2: Clinical characteristics of FSGS patients**
965

966 **Table S3: eQTL analysis of DNA repair genes in FSGS patients**
967 Ensg: ensemble gene ID; FDR: false discovery rate, PIP: posterior inclusion probability, AF:
968 allele frequency, beta: expression difference to reference allele
969

970 **Table S4: Full eQTL analysis of DNA repair genes in FSGS patients**
971
972